Regionally coupled atmosphere - ocean – sea ice – marine biogeochemistry model ROM. Part I: Description and validation.

Dmitry V. Sein[1,*], Uwe Mikolajewicz[2], Matthias Gröger[3], Irina Fast[4], William Cabos[5], Joaquim G. Pinto[6,7], Stefan Hagemann[2], Tido Semmler[1], Alfredo Izquierdo[8] and Daniela Jacob[9]

[1] *Alfred Wegener Institute, Bremerhaven, Germany*

[2] *Max Planck Institute for Meteorology, Hamburg, Germany*

[3] *Swedish Meteorological and Hydrological Institute, Norrköping, Sweden*

[4] *The German Climate Computing Center, Hamburg, Germany*

[5] *Department of Physics, University of Alcala, Alcala, Spain*

[6] *Department of Meteorology, University of Reading, Reading, United Kingdom*

[7] *Institute for Geophysics and Meteorology, University of Cologne, Cologne, Germany*

[8] *University of Cadiz, Marine Science and Technological Center of Andalusia, Cadiz, Spain*

[9] *Climate Service Center 2.0, Hamburg, Germany*

Key words: Regional climate model, OASIS, downscaling, REMO, MPIOM, coupled model, North Atlantic, Europe

* Corresponding author.
e-mail: dmitry.sein@awi.de

ABSTRACT

The general circulation models used to simulate global climate typically feature resolution too coarse to reproduce many smaller scale processes, which are crucial to determining the regional responses to climate change. A novel approach to downscale climate change scenarios is presented which includes the interactions between the North Atlantic Ocean and the European shelves as well as their impact on the North Atlantic and European climate. The goal of this paper is to introduce the global ocean – regional atmosphere coupling concept and to show the potential benefits of this model system to simulate present day climate. A global ocean – sea ice – marine biogeochemistry model (MPIOM/HAMOCC) with regionally high horizontal resolution is coupled to an atmospheric regional model (REMO) and global terrestrial hydrology model (HD) via the OASIS coupler. Moreover, results obtained with ROM using NCEP/NCAR reanalysis and ECHAM5/MPIOM CMIP3 historical simulations as boundary conditions are presented and discussed for the North Atlantic and North European region. The validation of all the model components, i.e. ocean, atmosphere, terrestrial hydrology and ocean biogeochemistry is performed and discussed. The careful and detailed validation of ROM provides evidence that the proposed model system improves the simulation of many aspects of the regional climate, remarkably the ocean, even though some biases persist in other model components, thus leaving potential for future improvement. We conclude that ROM is a powerful tool to estimate possible impacts of climate change on the regional scale.

1. Introduction

Numerical models are very effective tools to investigate the complex systems and associated mechanisms in climate and environmental sciences. Recently, much effort has been made to develop Earth System Models (ESMs) that include coupled representations of the ocean, atmosphere, land use, vegetation, biogeochemistry, atmospheric chemistry, and the hydrological cycle [Taylor et al., 2012]. ESMs can be used to simulate not only the longer term evolution of the Earth's climate on decadal and longer time scales but also to make short and medium-range weather forecasts and seasonal predictions. Still, ESMs have difficulties simulating weather and climate on regional and local scales. For example, limitations in computer power do not allow simulations with sufficient horizontal resolution to resolve key processes necessary for those spatial scales. The application of regional climate models (RCMs) is a valid possibility to improve on this drawback of current ESMs. RCMs take the initial conditions, time-dependent lateral conditions and surface boundary conditions from the global models and provide dynamically downscaled climate information within the region of interest. Additionally, they allow a better understanding of various aspects of air-sea interaction processes important for the climate.

There is a vigorous ongoing debate on whether RCMs can provide added value to GCMs in the context of determining the regional responses to climate change. This discussion relates primarily to the fact that climate is by its nature a large-scale phenomenon. Large-scale phenomena like the Inter Tropical Convergence Zone (ITCZ) or the monsoon circulation in the subtropics, or large-scale patterns of variability such as the North Atlantic Oscillation [Hurrel and Deser, 2009], are reproduced reasonably well in global climate models. The spatial extension of these phenomena and patterns is in most cases larger than the domain size of most RCMs. Historically, RCMs have been developed primarily to reproduce an observed climatology rather than to predict the regional responses to a changing climate [e.g. Kerr, 2013]. Still, Feser et al. [2011] could demonstrate an added value by analyzing different

regional atmospheric models for reanalysis hindcast simulations and simulations driven by climate model output. The added value originates mainly from the higher resolved orography in the RCMs, and the added value is larger for parameters exhibiting high spatial variability, such as near surface temperature [Feser et al., 2011].

To date, many RCMs have been composed of an atmospheric component coupled to a land surface scheme and driven over ocean areas by prescribed sea surface temperature (SST) and sea ice cover. Although these RCMs are sufficient for many applications, there are cases when fine scale atmosphere-ocean feedbacks can substantially influence the spatial and temporal structure of regional climate [Li et al., 2012]. Recent studies have shown that regional atmosphere-ocean climate models (RAOCMs) are capable of simulating these features of the climate system. For instance, Ratnam et al. [2008] found that coupling considerably improved the simulation of the Indian monsoon rain band over both the ocean and land areas. A similar result has been obtained by Li et al. [2010] in the simulation of East Asia monsoon precipitation. Aldrian et al. [2005] have shown that interactive calculation of SST with high spatial resolution leads to a significant improvement of the simulation of rainfall over Indonesia. Recently, a number of RAOCMs have been developed for studying the climate in the Mediterranean region, characterized by a complex morphology and strong air-sea interactions. Somot et al. [2008] coupled the global atmospheric model ARPEGE [Deque and Piedelievre, 1995] with the regional ocean model OPAMED [Somot et al., 2006] and studied the climate change signal in the Mediterranean. A similar development was conducted by Artale et al. [2009] with the PROTHEUS system, an atmosphere-ocean RCM for the Mediterranean basin. Dobrinski et al. [2012] developed MORCE (Model of the Regional Coupled Earth system), a coupled ocean-atmosphere with non-hydrostatic capabilities. Several regional coupled model systems have been developed to study interannual variability in the Arctic [e.g. Döscher et al. 2002, Rinke et al. 2003, Mikolajewicz et al. 2005, Sein et al., 2014].

Compared to global coupled atmosphere-ocean models, RAOCMs can achieve much higher resolution and detailed parameterizations, providing a more accurate representation of the morphological complexity of the land-sea contrasts and relevant small-scale processes. Compared to atmosphere and ocean only regional models, RAOCMs also give a dynamically and thermodynamically consistent representation of the SST, making the representation of interactions between the ocean and atmosphere more realistic than in atmosphere and ocean only regional models.

The development of RAOCMs can be traced back to the 1980s, when Zebiak and Cane [1987] coupled a Gill-type atmospheric model to a 1.5-layer oceanic model to study the ENSO phenomenon. Further evolution of regional coupled modeling progressed into two different directions. The first kind of coupled models focuses on short time scales [e.g. Pullen et al. 2006, Nichols and Toumi, 2013, Sanna et al., 2013]. Models of the second group (to which the RAOCM presented here belongs) are dedicated to the simulation of regional climate on time scales from several years to several decades. To our knowledge, the first fully coupled regional atmosphere/ocean/ice models for multi-year climate simulations were developed to simulate the Baltic Sea climate by Döscher et al. [2002] and Lehmann et al. [2004]. A more complete review of previous efforts in regional climate modeling can be found in e.g. Seo el al., [2007]

Here we introduce a novel approach to downscale climate simulations and to investigate the interactions between the North Atlantic and Arctic Ocean as well as the impact of ocean - atmosphere interaction processes on the regional climate. A global ocean – sea ice – marine biogeochemistry model with regionally high horizontal resolution is coupled to an atmospheric regional model and global terrestrial hydrology model. This technique of coupling divides global ocean model setup into two different subdomains: coupled, where the ocean and the atmosphere are interacting, and uncoupled, where the ocean model is driven by prescribed atmospheric forcing and runs in a so-called stand-alone mode. Therefore, choosing

a specific area for the regional atmosphere we can assume that in that area the ocean-atmosphere system is "free", whereas in the remaining areas the ocean circulation is driven by prescribed atmospheric forcing.

One of the main problems of RAOCMs is the prescription of lateral boundary conditions for the regional ocean models. Currently, global ocean reanalysis data sets (e.g. SODA [Carton and Giese, 2008], ECCO [Chen et al., 2014], HYCOM [Metzger et al., 2014], ORA [Balmaseda et al., 2013]) are available and are widely used as lateral boundary conditions for regional models; but they are mainly based on monthly means, damping the ocean dynamics on time scales less than one month. Additionally, regional climate models should effectively resolve the small-scale processes that are not adequately represented in the coarser model data used as boundary conditions. This creates inconsistencies between the regional model solution and the external data that can be avoided with the consideration of a global ocean model with refined resolution within the coupled domain. The use of a global ocean model also allows trapped coastal waves (originating from outside the coupled domain) to influence the barotropic sea level variability and the bottom pressure in the coupled domain. A shortcoming of the global ocean model arises from the fact that the model is forced with low resolution and lower-frequency atmospheric data outside the coupled region. Such atmospheric data is known to have biases, e.g., too weak wind speed in the tropics. This problem is not completely avoided by regional ocean models, because a typical ocean reanalysis which would be used as lateral boundary condition is generated by running ocean models forced by the same atmospheric reanalysis we use outside the coupled region.

Another important advantage of using a global ocean model appears when considering climate change scenario simulations for future decades. The regional ocean models have to implement lateral boundary conditions obtained from significantly coarser global AOGCMs scenario simulations, introducing biases in the results. The use of a gradually refined global ocean model coupled with a regional atmospheric model can thus provide more accurate

simulations both within and outside of the coupled area. Additionally, the use of monthly mean data obtained from global AOGCM climate change scenario runs as lateral boundary condition makes the investigation of possible long-term changes in some extreme events impossible (e.g. floods in the North Sea).

The goal of this paper is to introduce the global ocean – regional atmosphere coupling concept and to demonstrate the ability of this model system to simulate present day climate. Earlier versions of this model were used to study the effect of air–sea coupling on Indonesian rainfall [Aldrian et al. 2005], interannual variability of sea ice extent in the Arctic Ocean and "Nordic Seas" [Mikolajewicz et al. 2005], the influence of the choice of coupled area on the simulated Arctic climate [Sein et al. 2014] and simulation of the present climate and its future change in the region of the North Sea [Bülow et al. 2014, Su et al. 2014]. Using the global ocean model alleviates some well-known problems with oceanic boundary conditions, allows the investigation of the coupling feed-backs between coupled and uncoupled ocean areas [Sein et al., 2014] and provides an additional "degree of freedom" in the model setup and tuning, which can be helpful for example to adjust the ocean component for the better performance within the region of interest. For example the better Gulf Stream separation in the uncoupled area leads to a better representation of the Sub-Polar Gyre (SPG), which is located in the coupled domain and plays an important role for the cyclogenesis of extra-tropical cyclones over the North Atlantic basin. It should be noted that the ocean model is constrained by atmospheric forcing of the driving data (in our case reanalysis or ECHAM-MPIOM) outside the coupling area.

The paper is organized as follows. We introduce our coupled model and describe each of its components in section 2. In section 3, we present the setup of a coupled model simulation for the North Atlantic region, followed by the validation of the obtained results in section 4. Finally, section 5 gives our summary and conclusions.

2. Model components

Our coupled model comprises the REgional atmosphere MOdel (REMO), the Max Planck Institute Ocean Model (MPIOM), the HAMburg Ocean Carbon Cycle (HAMOCC) model, and the Hydrological Discharge (HD) model which are coupled via OASIS coupler. Note that all models except REMO are run in a global configuration.

From now on, we use for our REMO/MPIOM/HAMOCC/HD coupled model the acronym ROM (**R**EMO-**O**ASIS-**M**PIOM).

2.1. Ocean (MPIOM)

The oceanic component of ROM is the Max Planck Institute Ocean Model (MPIOM), developed at the Max Planck Institute for Meteorology [Marsland et al. 2003, Jungclaus et al. 2013]. MPIOM is a free surface, primitive equations ocean model which uses the Boussinesq and incompressibility approximations. The model is formulated on an orthogonal curvilinear Arakawa C-grid with z-level vertical discretization. The curvilinear grid allows for the placement of the poles over land, thus removing the numerical singularity associated with convergence of meridians at the geographical North Pole. An important advantage of the curvilinear grid is that high resolution in the region of interest can be reached, while maintaining a global domain. This avoids the problems associated with either open or closed boundaries in a regional ocean model.

The model has an embedded dynamic/thermodynamic sea ice model with viscous-plastic rheology based on Hibler [1979]. The thermodynamics relate sea ice thickness changes to a balance of radiative, turbulent and oceanic heat fluxes. The sea ice coverage is fractional within grid cells and is related to the thickness according to sub-grid scale parameterization of lateral versus vertical ablation and accretion following Stössel [1992]. The considerable

insulating effects of snow accumulation on sea ice are included, along with snow-ice formation when the snow/ice interface sinks below the sea level due to snow loading.

Several parameterizations of sub-grid scale processes are incorporated in the model. Firstly, a bottom boundary layer (BBL) slope convection scheme was included, which allows for a better representation of the flow of statically unstable dense water masses over sills and off shelves [Marsland et al., 2003]. Secondly, harmonic horizontal diffusion of the tracer fields has been replaced by an isopycnal scheme [Griffies, 1998]. Thirdly, eddy-induced tracer transport has been included by the implementation of a Gent and McWilliams style parameterization [Gent et al., 1995]. Fourthly, the deep convection is parameterized using enhanced vertical diffusion [Marsland et al., 2003].

The ocean tidal forcing in our model is derived from the full ephimeridic luni-solar tidal potential [Thomas et al., 2001]. The inclusion of the tides shortens significantly the ocean model time step. For an accurate temporal resolution of the tidal oscillations the ocean model time step has to be limited to 15-20 minutes. Even if the model stability criteria allow the use of larger time steps we have to keep in mind that for an accurate simulation of the barotropic oscillations they should be "represented" by about 50 time steps per period. In the case of coarse global climate models this restriction could be crucial. Taking the semi-diurnal tides (ca. 12 hours period) into consideration, the approximate time step in our model is about 15 minutes (one 50^{th} of 12 hours), thus satisfying this condition. As our ocean model set-up has much higher spatial resolution and, the required time step is therefore much shorter, the inclusion of the ocean tides does not substantially increase computational costs.

2.2. Atmosphere (REMO)

The atmospheric component of ROM is the REgional atmosphere MOdel (REMO) [e.g., Jacob, 2001]. The dynamical core of the model as well as the discretization in space and time, are based on the Europa-Modell of the German Weather service [Majewski, 1991]. The

physical parameterizations are taken from the global climate model ECHAM versions 4 and 5 [Röckner et al., 1996, Röckner et al. 2003]. REMO's prognostic variables are the surface pressure, horizontal wind components, temperature, water vapour, liquid water, and cloud ice. To avoid the largely different extensions of the grid cells close to the poles, REMO uses a rotated grid, with the equator of the rotated system in the middle of the model domain. The horizontal discretization is done on the Arakawa-C-grid and the hybrid vertical coordinates are defined according to Simmons and Burridge [1981]. The time discretization is based on the leap frog scheme with semi-implicit correction and Asselin filter smoothing.

For ocean grid points, sea surface temperature and sea ice distribution are prescribed as lower boundary values. The seasonally varying vegetation parameters like the vegetation ratio, the forest ratio and leaf area index are described by Rechid and Jacob [2006]. All prognostic variables except for the liquid water and cloud ice are relaxed towards the forcing data in the outer eight rows of the model area according to lateral boundary conditions formulated after Davies [1976]. At the upper boundary a radiative upper boundary condition following Klemp and Durran [1983] and Bougeault [1983] is applied. The radiation parameterization is adopted from the European Centre for Medium Range Weather Forecasts' model [Fouquart and Bonnel, 1980; Morcrette and Fouquart, 1986] with changes for ECHAM4 described in Roeckner et al. [1996].

Clouds are divided into stratiform and convective clouds. The liquid water and ice content of stratiform clouds are determined by the corresponding budget equations including sources and sinks due to phase changes and precipitation. The parameterizations of cloud processes are taken from the ECHAM5 model [Roeckner et al., 2003]. The parameterization of the convective clouds is based on the mass flux concept from Tiedtke [1989] with modifications of the adjustment closure for deep convection according to Nordeng [1994]. Soil temperatures on land are calculated from diffusion equations solved in five different layers covering the uppermost 10 m of the soil. For the soil hydrology, three different budget equations for the

amount of snow, the water intercepted by vegetation and the soil water content are applied. The surface temperature of the sea ice is determined from the residual of the heat and radiation fluxes at the ice surface. Snow on sea ice is not explicitly considered in REMO but is indirectly accounted for by the sea ice albedo and the calculation of the conductive heat flux through the ice as an addition to the ice thickness. In our case, snow over the sea ice is accumulated and melted in MPIOM, which "receives" snow fall from REMO, and returns the effective sea ice – snow thickness and snow cover mask to REMO. The sea ice albedo is assumed to depend on the surface temperature and has values between 60% and 80%. If snow is present, this range is shifted to 65% - 85%.

REMO has a fractional specification for land, water and sea ice in one grid cell [Semmler et al. 2002]. At the surface, fluxes, temperature and humidity are computed separately for each surface type, according to Avissar and Pielke [1989]. The surface fluxes are averaged over the three different surface types (weighted by the respective fractional area) to determine the effects of the fluxes on temperature and humidity in the lowest model level. In all other model levels, each value for the fluxes, temperature and humidity is representative for the whole box. The model characteristics are described in more detail in Jacob [2001], Jacob et al. [2001] and Deque et al. [2007].

2.3. Marine biogeochemistry (HAMOCC)

The HAMburg Ocean Carbon Cycle model HAMOCC [Maier-Reimer, 1993, Maier-Reimer et al., 2005] includes the relevant carbon stocks of the atmosphere, the ocean, and the sediments and simulates the exchange between them. The model receives temperature and salinity fields from MPIOM to compute the transformation rate constants as required for the air sea gas exchange, whereas tracer advection and diffusion is determined by MPIOM. Shortwave radiation at the top of the water column is given as an atmospheric forcing field to simulate photosynthesis which is limited by phosphate, nitrate, and Fe. A detailed model

description and validation of the model's mean biogeochemical state is given in Wetzel [2005].

Modifications have been made for the current study to take the specific conditions in shallow marine semi-enclosed shelf seas into account. These comprise the implementation of a new light penetration scheme for the biogeochemical model, including light attenuation due to silt near the coasts [Heath et al., 2002; Paetsch and Kuehn, 2008], and the implementation of river loads of dissolved nutrients and other chemical elements [Maybeck and Ragu, 1997]. Details can be found in Gröger et al., [2013].

HAMOCC simulates the cycle of Nutrients, Phytoplankton, Detritus, and Zooplankton (NPDZ model). It has three basic productivity limiting nutrients (PO_4, NO_3, Fe). The growth rate of phytoplankton is limited by photosynthetic active radiation, which is calculated from shortwave radiation at the surface. Light is further attenuated with depth by water turbidity and the self-shading by phytoplankton. Only one phytoplankton prognostic state variable is calculated from which opal and calcite shells are computed separately. In the global ocean this approach reflects largely the production of Coccolithophorids, flagellates, and diatoms. The latter group is assumed to grow fastest when sufficient silicate is available. Grazing by zooplankton is modelled by a simple Monod function using a maximum growth rate (or grazing rate) and a half saturation constant. Zooplankton is further diminished by a constant death rate (parameterizing the effect of predators) and a mortality rate. The latter is immediately remineralized. Additionally, a third biomass pool of Dissolved Organic Matter (DOM) exists which is fed by phytoplankton and zooplankton excretion. Dead phytoplankton (detritus) as well as carbonate and opal shells fall down to the bottom with different constant velocities. However, aggregation processes are not accounted for. If enough oxygen and dead phytoplankton (detritus) is available, DOM is remineralized at constant rates. In the absence of oxygen, denitrification takes place by bacteria which are not modelled explicitly. Opal and carbonate shells are likewise dissolved at constant rates. The inorganic carbon cycle is

represented by dissolved inorganic carbon (DIC) and total alkalinity (TA). During phytoplankton production, DIC is reduced, which lowers the air sea pCO_2 difference at the ocean surface. Correspondingly, calcite production (dissolution) within (below) the euphotic zone reduces DIC. Thus, the model simulates the oceanic carbon pump and carbonate pump. At the bottom, the model is closed by a 12 layer sediment module [Heinze et al., 1999], which simulates pore water chemistry and which is in diffusive exchange with the bottom layer. The air-sea gas exchange for CO_2, O_2, and N_2 is parameterized using the Schmidt number and piston velocity according to Wanninkhof [1992]. The temperature dependence of the Schmidt number has been adapted according to the recommendation of Gröger and Mikolajewicz [2011]. A full technical description of the model is available in Maier-Reimer et al. [2005].

2.4. River runoff (HD)

The Hydrological Discharge (HD) model [Hagemann and Dümenil 1998; Hagemann and Dümenil Gates, 2001] simulates globally the lateral freshwater fluxes at the land surface. It is a state-of-the-art discharge model that is applied and validated on the global scale, and it is also part of the coupled global AOGCM ECHAM5/MPIOM [Roeckner et al., 2003; Jungclaus et al., 2006]. As a general strategy, the HD model computes the discharge at 0.5° resolution with a daily time step. In the HD model, the lateral water flow is separated into the three flow processes: overland flow, base flow and river flow. The overland flow uses surface runoff as input and represents the fast flow component within a grid box, the base flow is fed by drainage from the soil and represents the slow flow component, and the inflow from other grid boxes contributes to river flow. The sum of the three flow processes equals the total outflow from a grid box. The model parameters are functions of the topography gradient between grid boxes, the slope within a grid box, the grid box length, the lake area and the wetland fraction of a particular grid box. More details can be found in model Hagemann and Dümenil [1998] and Hagemann and Dümenil Gates [2001].

2.5. Coupling

REMO/MPIOM coupling was carried out using the OASIS coupler developed by CERFACS [Valcke et al., 2003]. The coupling procedure is similar to the one used in the MPI climate models ECHO-G [Legutke and Voss, 1999] and ECHAM5/MPIOM.

Momentum, heat and freshwater fluxes are calculated in the atmosphere model for the open water and ice covered part of the grid box separately:

$$Q^W = Q^W_{SW} + Q^W_{LW} + Q^W_S + Q^W_L \quad (1)$$

$$Q^I = Q^I_{SW} + Q^I_{LW} + Q^I_S + Q^I_L + Q^I_C + Q^I_R \quad (2)$$

where upper indices denote the fluxes over open water (W) and the fluxes over ice (I). Lower indices indicate net shortwave radiation (SW), net long wave radiation (LW), sensible (S) and latent (L) heat fluxes. There are two additional sources for the ice-covered part, namely the conductive heat flux (Q^I_C) which is responsible for the ice growth, and the residual heat flux (Q^I_R), which is used to melt ice. Conductive heat flux through the snow/ice layer is defined as:

$$Q^I_C = \frac{k_I}{h_{eff}} \cdot (T^I - \theta)$$

where T^I is the snow/sea ice skin temperature, θ the temperature at the ice-water interface, i.e. freezing temperature, h_{eff} the effective ice thickness defined as $h_{eff} = (k_I \cdot h_S + k_S \cdot h_I)/k_S$, with k_I and k_S being the heat conductivities of ice and snow and h_I and h_S the ice and snow thickness respectively. A detailed description of the calculation of fluxes used in (1)-(2) can be found in Roeckner et al. [2003] and Legutke and Voss [1999]

Freshwater fluxes are separated in liquid (W) and solid (I) parts:

$$P^W = P_T - P_{SN} + E^W \quad (3)$$

$$P^I = P_{SN} + E^I \quad (4)$$

where P_T is total precipitation, P_{SN} snow fall, E^W surface evaporation, and E^I sublimation of sea ice. Dynamical forcing of the ocean model is represented by wind stress and sea level pressure (SLP). Wind stress is calculated separately for open water and sea ice. We use the standard formulation of the wind stress, i.e. its quadratic dependence on the wind velocity relative to the ocean surface velocity. The difference between wind stress over sea ice and over water is given by the drag coefficient, i.e. the surface roughness. Whereas surface roughness for the open water is calculated from the Charnock formula [Charnock, 1955], sea ice roughness is constant and set to 1 mm in our simulations. For the partially ice covered regions wind stress is calculated as weighted mean of the contributions of wind stress over ice and water.

The effect of ocean surface currents is taken into account for the calculation of turbulent fluxes. The wind velocity relative to the ocean surface (sea ice) velocity |**W**-**u**| is used, rather than the absolute near surface wind speed |**W**| (**u** is the ocean surface or sea ice velocity). This modification is important given strong ocean tides and in model configurations with relatively high spatial resolution [e.g., Dawe and Thompson, 2006], which is the case for our set-up.

As the regional model (REMO) covers only a part of the global ocean, MPIOM needs to be run in both coupled (the branch REMO – OASIS – MPIOM, Fig.1) and stand-alone (the branch External Forcing - Bulk Formulae - MPIOM, Fig.1) modes simultaneously. The ocean model running in the coupled sub-domain receives the heat, freshwater and momentum fluxes calculated in REMO (F_{REMO}) at specified frequency (coupling time step) and passes the sea surface conditions to the atmospheric model. In the uncoupled sub-domain, the ocean model calculates heat, freshwater and momentum fluxes (F_{Bulk}) from the global, predefined atmospheric fields (e.g. from reanalysis data) using bulk formulas (see Fig.1 External Forcing - Bulk Formulas – MPI-OM) at specified frequency (forcing time step). A detailed description

of the bulk formulas used to simulate the fluxes in the uncoupled domain can be found in Marsland et al. [2003]. Note that the coupled time step and the forcing time step can be different. The resulting fluxes used as ocean forcing (F_{Ocean}) are a combination of F_{REMO} and F_{Bulk}:

$$F_{Ocean} = \chi F_{REMO} + (1-\chi) F_{Bulk} \tag{5}$$

where χ is a smooth transition coefficient changing from 1 inside the REMO domain to 0 outside. The fluxes F_{REMO} are calculated in the atmospheric model according to equations (1) - (4).

Interpolation from the atmospheric grid to the ocean grid and vice versa is done in the ocean model using the so-called mosaic approach, which can be briefly described as follows:

$$F_{ij}^{MPIOM} = \frac{\sum_{lm} F_{lm}^{REMO} \cdot A_{ijlm}}{\sum_{lm} A_{ijlm}} \quad ; \quad F_{lm}^{REMO} = \frac{\sum_{ij} F_{ij}^{MPIOM} \cdot A_{ijlm}}{\sum_{ij} A_{ijlm}} \tag{6}$$

where F_{ij}^{MPIOM} and F_{lm}^{REMO} are the values of F in the ocean grid box *(i,j)* and atmosphere grid box *(l,m)* respectively. A_{ijlm} is interpolation (weight) matrix, defined as a common surface area between ocean grid box *(i,j)* and atmosphere grid box *(l,m)*.

Thus, the OASIS coupler "sees" both models on the same computational grid, i.e. REMO grid. Due to the smaller spatial scales of oceanic processes, ocean models usually have a higher spatial resolution than atmospheric models. To provide the adequate atmospheric feedback for small scale SST anomalies, a sub-scale correction of the atmospheric heat fluxes is applied. As these fluxes strongly depend on sea surface temperature (SST), this correction is assumed to be proportional to the difference between the SST calculated in MPI-OM and the same SST interpolated onto the atmospheric grid and backward. The proportionality constant which is equal to $\partial Q/\partial T$, where Q is a heat flux and T is a sea surface temperature, was set according to Roeske [2001] to 30 $W/(m^2K)$. Note that the value of 30 $W/(m^2K)$ is obtained for the northern North Atlantic. For different ocean regions its annual mean varies

from ~20 $W/(m^2K)$ in polar regions to ~65 $W/(m^2K)$ in tropics [Roeske, 2001]. Sensitivity studies with $\partial Q/\partial T$ set to 20 $W/(m^2K)$ and 40 $W/(m^2K)$ showed that the differences to the results obtained with 30 $W/(m^2K)$ were negligible. Because both the SST interpolations (forward and backward) are linear (see eq. 6), and sub-scale heat flux correction linearly depends on SST, the mean sub-scale heat correction over the coupled domain is zero. In other words, this term only redistributes atmospheric heat over smaller ocean grid cells but does not change the integrated heat balance.

REMO requires surface temperature not only over the sea, ice or land, but also over inland lakes, which are not represented in the ocean model. Lake surface temperature (LST) is calculated using the following simplified procedure: all lakes are assumed to be well mixed and to have constant depth of 20 m. The atmospheric heat fluxes over the water in the grid box, where lakes are present, are added to the lake‘s heat content. If the resulting heat content is positive the lake temperature (which is assumed to be equal to the LST) is calculated from its value. If heat content becomes negative it is set to zero and the energy is used to form ice. In our model we do not consider the case when all water of the lake is frozen. However, this possibility is not realistic under present climate conditions for a 20 m lake depth.

The Hydrological Discharge model is coupled to both the ocean and the atmosphere model with 24 hours frequency. It receives the surface runoff and drainage from REMO and delivers the freshwater river inflow to MPIOM. In regions covered with glaciers, which are prescribed in our model explicitly, the total precipitation is provided into the HD model. The freshwater inflow into the ocean is then calculated assuming an artificial river flow (instead of glacier flow). The replacement of the glacier flow by river flow is a simple assumption, but it allows us to close the freshwater balance over the glaciers.

3. Experimental Setup.

In order to evaluate and validate the North Atlantic climate as simulated by ROM, we now analyse and compare the output of two ROM simulations carried out with the same set-up (as described in section 2) but with different atmospheric forcing. For the first simulation (ROM-NCEP), atmospheric data from the NCEP/NCAR reanalysis [Kistler et al., 2001] for the period 1948-2007 is used as boundary conditions. For the second run (ROM-ECHAM5), the boundary conditions are taken from a 20th century simulation (1920-2000) with the ECHAM5/MPIOM AOGCM performed in the framework of the CMIP3 [Roeckner et al., 2006].

3.1 REMO/HD setup

The computational grid of the atmospheric model REMO used in this study has about 37 km horizontal resolution and 27 hybrid vertical levels. It covers all of Europe and parts of the Arctic and the North Atlantic (Fig.2). The model is run with ECHAM4/ECHAM5 physics. Initial and lateral boundary conditions are obtained from the same data set used for MPIOM forcing in uncoupled domain (see 3.2), i.e. NCEP reanalysis [Kistler et al., 2001] or ECHAM5/MPIOM IPCC C20 simulations [Roeckner et al., 2006]. REMO obtains the lower boundary conditions over the sea and sea ice surfaces from MPIOM through the OASIS coupler every coupled time step. Simultaneously, it provides the atmospheric momentum, heat and water fluxes to the ocean model. The Hydrological Discharge model has a global set-up and, thus also requires the surface runoff and drainage input outside the REMO domain (Fig.1, branches "External forcing-HD-MPIOM"). This data was either taken from the corresponding global driving atmospheric model (ECHAM5/MPIOM in the case of scenario simulations) or generated using the MPI-M Hydrology Model [MPI-HM; Stacke and Hagemann, 2012] driven by the Watch Forcing Data [Weedon et al., 2011] for the NCEP hindcast runs. Both the surface runoff and the drainage obtained from REMO are interpolated

onto the HD grid, merged into the corresponding global data set and used as forcing in the HD model.

3.2 MPIOM setup

The particular MPIOM set-up used in this study has high resolution in the North Atlantic and in the North European shelves. The horizontal resolution gradually varies between a minimum of 5 km in the North Sea (Fig.2) and a maximum of 220 km in the Antarctic (not shown). The model has 30 vertical levels with increasing level thickness, i.e. 16, 10, 10, 10, 11, 13, 16, 19, 23, 23, 28, 33, 40, 48, 58, 70, 84, 102, 122, 148, 178, 214, 258, 311, 375, 452, 544, 656, 791, 800 m. The thickness of the first model layer (16 m) was chosen to ensure model stability. As the MPIOM does not support drying, the thickness of the upper model layer has to be larger than maximal tidal amplitude plus maximal sea ice thickness. The density ratio between sea ice and sea water was considered for this calculation.

The North Sea – Baltic Sea system was treated differently than the other oceans. The sea ice salinity in the Baltic Sea was set to 0 (instead of 5 for ocean sea ice). This was done because the minimum salinity in the Baltic Sea waters can be close to 0, and the Baltic Sea ice salinity reflects the low water salinities [Granskog et al., 2006]. The bottom topography of the Danish straits was corrected to provide realistic exchange between the North and the Baltic Seas. Narrow and deep trenches with a width of several hundreds of meters and a depth of up to 50 m play an important role for this exchange [She et al., 2007]. It is clear that we cannot resolve such trenches with a global ocean model. For this reason, the bottom topography in the straits is set as follows: (i) at least one grid box width across the strait and (ii) three active layers, i.e. the minimal depth is 36m. Three is a minimal number of layers in a z-coordinate model, which could simulate more or less realistic exchange flow through the shallow strait. In stand-alone mode, MPIOM is started with climatological temperature and salinity data [Levitus, 1998]. It is integrated four times through the 1948-2000 period using 6 hourly

NCEP reanalysis data as forcing. Each individual run uses the end of the previous run as the initial condition.

With the ocean model running uncoupled (i.e. in stand-alone mode), an inconsistency in fresh water budget arises. While precipitation and river runoff are prescribed from reanalysis or observational data, surface evaporation is calculated by the model. To avoid the model drift caused by this inconsistency, a salinity-restoring correction is applied also to the natural freshwater fluxes. This correction is implemented by adding an additional "source" term of the form $-(S-S_{obs})/k$ to the advection-diffusion salinity equation. Hereby S is the modelled salinity, S_{obs} is the "observed" salinity to which the computed salinity should be restored, and k is a time constant regulating the restoring speed. The details of the salinity-restoring algorithm implemented in MPIOM are described in Marsland et al. (2002). In our simulations, restoring was performed for the surface layer (0–16 m) towards Polar science center Hydrographic Climatology (PHC) [Steele et al., 2001] with a time constant of 180 days. No salinity restoring is applied under sea ice.

The global climatology does not realistically represent the low salinities in river plumes and estuaries. To avoid unrealistically strong restoring towards too high salinities in river mouths, restoring was switched off in regions where surface salinity was less than 28 by applying a smooth transition coefficient changing from 0 ($S<28$) to 1 ($S>30$). To avoid an unrealistically large restoring, the absolute value of the difference $|S-S_{obs}|$ was restricted to 1.

In coupled mode, the model is started from the final state reached in the last standalone run. The initial date is 01.01.1948 for NCEP forced runs and 01.01.1920 for ECHAM5/MPIOM forced simulations. An earlier starting date for the ECHAM5/MPIOM forced run was chosen because of the ocean biogeochemical spin-up (see 3.3). Forcing time step was 6 hours and coupling was done hourly.

For both the NCEP and ECHAM5/MPIOM forced simulations, two subsequent coupled model integrations were carried out. In the uncoupled domain, inconsistencies in the

freshwater budget over the ocean were leading to a substantial drift of the model. To overcome this, salinity in the surface layer (0–16 m) was also restored in the first coupled integration in the ice-free regions towards climatology in ROM-NCEP, and towards climatology plus anomalies of the ECHAM5/MPIOM model in ROM-ECHAM5. The time constant of 180 days was used as in the uncoupled simulations. In subsequent experiments, the restoring was switched off and a temporally-constant freshwater flux correction was used instead. This was calculated for the period 1970 to 2000 from the first coupled integration. We focus on the 1970 - 2000 period because the years before 1969 were considered to be a transition period from the uncoupled to the coupled state. The advantage of the temporally-constant freshwater flux correction is the preservation of the interannual variability. On the other hand, the restoring term corrects the sea surface salinity towards climatology, thus strongly reducing the possible drift. The necessity for additional model runs for obtaining temporally-constant freshwater flux corrections is one of the disadvantages of the current approach. It should be noted that the salinity restoring and freshwater flux correction were switched off in both the North Sea and the Baltic Sea.

3.3 HAMOCC setup

The ocean biogeochemistry requires much longer spin-up than ocean dynamics. This fact makes it almost impossible to spin up the biogeochemical part of the model on the highly resolved computational grid. Therefore, we ran MPIOM/HAMOCC for several thousand (>4000) years using a two times coarser grid and preindustrial forcing obtained from ECHAM5/MPIOM IPCC simulations [Gröger et al., 2013].

The spin-up run was carried out without tides. These permits running the model with a longer time step. The prescribed atmospheric pCO_2 was set to 278 ppm (corresponding to the year 1765). The target for this run was to obtain air – sea CO_2 fluxes varying around zero. The last hundred years of this run were integrated with enabled tides. Further 95 years were run

with gradually increasing the atmospheric pCO_2 to 288 ppm (corresponding to year 1860). Subsequently, this run was integrated until 2100 with atmospheric pCO_2 following the A1B scenario (Fig. 3, black curve). Additionally, another run was initialized without climate warming but forced with the CMIP3 preindustrial forcing fields and with constant pCO_2. This run was carried out to ensure that the model has no substantial model drift. Unfortunately, this run was initialized accidentally with an atmospheric pCO_2 of 278 ppm instead of 288 ppm, so that the carbon cycle cannot be assessed. However, nutrient budgets are not strongly affected by the accidental perturbation in atmospheric pCO_2 and can thus be examined for potential model drifts.

Fig. 4 shows concentrations for dissolved nitrate averaged over a large part of the North Atlantic. The North Atlantic shows a trend towards slightly lower nutrient concentrations. These trends can be seen across all depth levels, which indicate that it is not a simple vertical nutrient redistribution in the water column but rather redistribution within the world ocean. However, the loss is only about 2% over the 240 years of integration. Thus, the model can be considered to be in approximate equilibrium.

After the preindustrial period the coarser MPIOM/HAMOCC was run up to year 1920. The HAMOCC state obtained for 01.01.1920 was then interpolated to the finer oceanic grid. Starting from this date, the model simulations were carried out on the fine (original) configuration. In the shallow North Sea, all biogeochemical tracers adapt very rapidly to the finer resolution so that spin-up effects are only identified for the first few years after 1920. However, spin-up effects must be expected to act for longer in the carbon cycle. Fig. 3 illustrates the time evolution of the total ocean carbon uptake in the two model setups. The coarse and the fine model configurations show similar results from 1970 onwards. Therefore, we here consider the first 50 years (1920-1970) as a “transition spin-up” for the ocean biogeochemistry. Table 1 shows that the rates of carbon uptake are well within the range of other published values [e.g. Orr et al., 2001; Le Quere et al., 2009; Ilyina et al., 2013].

Because NCEP forced simulations were started from 01.01.1948 they used HAMOCC initial conditions obtained from ECHAM5/MPIOM forced run for the corresponding date.

4. Comparison with observational data

In this section we present a selection of key fields from the period 1980-1999 and compare them to gridded data from different sources. These data sets are derived from observations or reanalysis datasets where appropriate. The period 1980-1999 was chosen for model validation because HAMOCC is still experiencing some adjustment before the 1980s (cf. section 3.3.).

4.1 Atmosphere

In this sub-section, the atmospheric component of the North Atlantic climate as simulated by ROM is evaluated. Among the pertinent variables, the mean sea level pressure (MSLP) is a good indicator for a realistic simulation of the large-scale circulation which influences near surface temperature (T2M) and precipitation distributions. Erroneous MSLP gradients induce an erroneous regional wind circulation [e.g. Hueging et al., 2013], and can also have a strong effect on ocean circulation. Figure 5 displays results for MSLP for the boreal winter, defined as December, January, and February (DJF) and summer, defined as June, July, and August (JJA). The values from ERA-Interim reanalysis (Fig. 5a,e) are used for comparison. ROM-NCEP provides the best agreement when compared to ERA-Interim. This is to be expected since REMO is driven by NCEP reanalysis data at the lateral boundaries, as opposed to ECHAM5 GCM data which are not constrained by observations. Deviations from ERA-Interim MSLP (Fig. 5b,f) are within 2 hPa over most of the domain for both seasons. The largest departures are found for DJF, when negative biases occur over an area reaching from the North Sea to the Caspian Sea (up to 3 hPa). These small MSLP differences can be partially attributed to differences between NCEP and ERA-Interim reanalyses, and to biases

occurring within the REMO model domain due to the model formulation. They imply comparatively small differences in terms of regional wind circulation. In summer, the ROM-NCEP MSLP is closer to ERA-Interim, with the largest positive departures located over Scandinavia. The anomalies over Greenland can be attributed to extrapolation effects below high orography.

The biases are much stronger for the ROM-ECHAM5 simulation, especially for DJF. A high pressure anomaly is identified at higher latitudes, extending from Greenland to the Kara Sea, while a low pressure anomaly extends from the British Isles to the Black Sea. These MSLP biases come primarily from the ECHAM5/MPIOM simulation (Fig. 5d,f) and their magnitudes are modified by REMO: for example, the positive MSLP anomaly over the Kara Sea in DJF is moderated in REMO-ECHAM5, while the negative anomaly over the British Isles and Central Europe is exacerbated in REMO-ECHAM5 (Fig. 5c,d). While the anomalies for JJA are weaker, the negative MSLP anomaly over northern Scandinavia is also enhanced by REMO (up to 6 hPa, cp. Fig. 5g,h). The changes of MLSP imply a reduction of the meridional MSLP gradient in DJF, and an enhanced north-south pressure gradient over continental Europe in JJA, thus leading to considerable changes in the near surface winds.

The identified MSLP biases are an indication of deficiencies in the representation of the large-scale atmospheric circulation. In order to analyse this in more detail, we now consider winter storm track variability and blocking frequencies for both summer and winter. The storm track variability is quantified as the standard deviation of 500 hPa geopotential for a time window from 2 to 8 days. This variable is a rough quantification of the combined intensities and frequencies of low-pressure and high-pressure systems and thus of synoptic activity [e.g. Hoskins and Valdes, 1990]. As in this frequency window the variability is dominated by low pressure centres, the storm track intensity is primarily a measure for cyclone activity. The blocking frequencies are computed from 500 hPa geopotential height fields for reference latitude of 60°N following the approach of Tibaldi and Molteni (1990).

For areas where the ROM data is not available, the corresponding information from NCEP or ECHAM5 is used for the computations. Therefore, the ECHAM5/MPIOM and ROM-ECHAM5 statistics are very similar except for the longitudes correspondent to the coupled model domain. Given the excellent agreement of 500 hPa geopotential fields for NCEP and ERA-Interim (not shown), the same is true for ERA-Interim and ROM-NCEP (cf. Fig. 5).

The ROM-NCEP storm track has a spatial structure and amplitude that closely resembles that of ERA-Interim (Fig. 6a,b), although small differences are noted: for example, the area of high variability extends further into the North Sea, Scandinavia and Eastern Europe in ROM-NCEP. On the other hand, the storm track variability for ROM-ECHAM5 is generally weaker than in ERA-interim (Fig. 6c). Over Europe, the storm track is displaced to the south, which is consistent with the southwards displaced MSLP gradient. These biases can also be found in ECHAM5/MPIOM (Fig. 6d, also Pinto et al., [2007]; their Fig. 1).

Fig 6e shows the DJF blocking frequencies for the different datasets as a function of longitude. The blocking frequencies for ROM-NCEP (red curve) are somewhat reduced over the study area (60°W – 60°E) compared to ERA-Interim (black curve). Both the ROM-ECHAM5 (purple curve) and ECHAM5/MPIOM (blue curve) show much lower blocking frequencies for this area, and it is clear that blocking biases are exacerbated in ROM-ECHAM5. This is in line with the above described MSLP anomalies. For the summer, the result is somewhat different: ROM-NCEP overestimates the frequency of blocking compared to ERA-Interim for the study area (60°W – 60°E), while ROM-ECHAM5 actually compensates a part of the strong negative bias in ECHAM5/MPIOM. In both cases, these results are in line with the above described MSLP and winter storm track changes, and document the interesting effect that the regional model may reduce or enhance the biases of the GCM depending on the season.

The results described above have implications for regional climate, in particular for the near surface (2 meter) temperature (T2M). Figure 7 shows the differences between ROM and

ERA-Interim for DJF and JJA. For ROM-NCEP, the winter departures are typically below 3 K over most of the coupled domain, except for the Barents and Kara Sea area, as well as east of Greenland (Fig. 7b), consistent with corresponding sea ice thickness biases (see section 4.3 and Fig. 19b). Over Europe, the departures are generally within 2 K, except for the Alpine region and an area between the Caspian and the Black Sea. Those differences can be partially attributed to differences in topography resolution.

The ROM-NCEP summer departures from ERA-Interim are generally below 2 K all over Europe and over most of the North Atlantic (Fig. 7f), but shows higher discrepancies over mountainous areas. The comparatively large biases between the Black and the Caspian Sea during summer could be related to deficiencies in the soil model as well as differences in the topography. The Baltic Sea also shows a negative bias.

ROM-ECHAM5 shows a distribution of T2M biases that resembles that of the ROM-NCEP simulation, but partly with stronger, partly with weaker anomalies. ROM-ECHAM5 shows much stronger negative anomalies in winter compared to both ROM-NCEP and ECHAM5/MPIOM, which extend from Scandinavia into Russia (Fig. 7c compared to Fig. 7b and 7d). The T2M east of Greenland, from Iceland to Svalbard, and over the Barents Sea is strongly reduced, reversing the ECHAM5/MPIOM warm bias and increasing the ROM-NCEP cold bias east of Greenland. The SST anomalies over the North Atlantic have a strong influence on the large-scale atmospheric circulation, as the storm track location tends to be co-located with the areas of stronger meridional SST temperature gradients due to the local maximum of low-level baroclinicity. The different blocking frequencies (Fig. 6e) and the more extensive sea-ice cover east of Greenland (section 4.3 and Fig.19) could also be partially associated with these differences. In summer, the deviations of ROM-ECHAM5 have a similar pattern to ROM-NCEP but the temperature is typically lower, increasing the ROM-NCEP cold biases(Fig. 7f,g). This could be explained by the stronger north-south pressure gradient (Fig. 5f,g) and the associated anomalous westerly flow and stronger maritime

influence, and the reduced blocking frequencies over Eastern Europe (Fig. 6f), as blocking situations in summer are associated with enhanced T2M values. Compared to ECHAM5/MPIOM (Fig. 7h), the reversal of the slight warm bias over the north-eastern North Atlantic is noteworthy. This could be due to changed ocean circulation connected with higher ocean model resolution (see section 4.3). Furthermore, the cold bias over Eastern Europe is reduced in ROM-ECHAM5 compared to ECHAM5/MPIOM.

4.2 Precipitation and river runoff

The simulated total precipitation (Fig. 8) is generally overestimated in both ROM simulations over large parts of Europe, particularly for ROM-ECHAM5. This overestimation is partially due to an overestimation of the hydrological cycle in REMO, although small areas with pronounced topography such as Scotland, the mountain range in the west of Norway and some parts of the Alps stand out with negative biases. The strong biases close to the REMO lateral boundary relaxation area are a computational artifact. Within the model domain, the biases should be partially related to temperature biases (Fig. 7c,d), as the amount of precipitable water in the atmosphere is primarily a function of temperature. The enhanced precipitation in ROM-ECHAM5 compared to both ROM-NCEP and ECHAM5/MPIOM in winter over Western Europe (Fig. 8b,c,d) is also associated with the southward displacement (compared to ROM-NCEP) or strengthening (compared to ECHAM5/MPIOM) of the storm track (Fig. 6b,c,d), thus bringing moist maritime air masses primarily towards this region. In summer, the ROM-ECHAM5 simulation shows more precipitation (Fig. 8g) compared to ROM-NCEP (Fig. 8f) south of Greenland, which should be primarily related to the temperature bias in ECHAM5 in the same area (Fig. 7g,h). The increase of precipitation and decrease of temperature over Continental Europe should be related with the too strong north-

south pressure gradient and the associated stronger maritime influence in ROM-ECHAM5 (Fig. 5g,h).

In order to evaluate the seasonal behavior of ROM and the added value of the downscaled precipitation, we consider spatial averages over several large catchments located within the regional domain (Fig. 9). For precipitation observations over land, we use the WATCH forcing data [WFD; Weedon et al. 2011]. Its monthly mean observed characteristics are taken from the Global Precipitation Climatology Centre full dataset version 4 (GPCC); [Fuchs et al., 2007]. This data set is corrected for gauge-undercatch following Adam and Lettenmaier [2003], i.e. the systematic underestimation of precipitation measurements that have an error of up to 10-50% (see, e.g. Rudolf and Rubel, [2005]).

Fig.10 shows that the NCEP summer precipitation is too large over all catchments. The overestimation of summer precipitation over most parts of the Northern Hemisphere is a known feature of the NCEP reanalysis [e.g. Hagemann and Dümenil Gates, 2001]. This overestimation is strongly reduced in the ROM-NCEP simulation. Moreover, the underestimated precipitation values for the other seasons are also reduced. This clearly indicates that the improved precipitation is an added value of ROM. For ROM-ECHAM5, the added value is spatially more variable. Over the Danube and Rhine rivers, an added value is provided as the so-called “summer drying problem” of ECHAM5/MPIOM is strongly reduced in ROM-ECHAM5. The problem is characterized by a too dry and too warm simulation of the summertime climate over central and Eastern Europe and is often reported for global and regional AGCMs [Hagemann et al., 2009]. Over the Baltic Sea catchment, ROM-ECHAM5 precipitation is closer to WFD data than ECHAM5/MPIOM from January- April, while it is somewhat worse in August and September. A similar behavior can be seen for the Elbe catchment. For both North Eastern European catchments (Northern Dvina and Volga), ROM-ECHAM5 largely overestimates precipitation in summer and autumn, while

ECHAM5/MPIOM is comparatively close to the WFD data, so that the downscaling provides no added value in this case.

The discharge simulated by the HD model captures the observed seasonal cycles of discharge quite well (Fig.11). Usually deficiencies in simulated precipitation are propagated into discharge, which shows analog biases: overestimation for Baltic Sea, Northern Dvina, Volga (both ROM-NCEP and ROM-ECHAM5), Elbe and Rhine (only ROM-ECHAM5), underestimation for Danube (especially ROM-NCEP). E.g. for the Baltic Sea catchment precipitation is 11-14% larger than WFD data, which leads to a 23-31% overestimation of river runoff into the sea for ROM-NCEP and ROM-ECHAM5, respectively. Nevertheless, the seasonal cycle of the total river runoff into the Baltic Sea is captured well representing the maximum in May and two local minima in February and September. The snow melt induced discharge peaks for Baltic Sea, Northern Dvina and Volga are well timed, but for the latter two catchments the decreasing flank is delayed due to the overestimated precipitation. This is particularly the case for the Volga, where the simulated maximum discharge is delayed by one month.

4.3 Ocean and sea ice

The comparison between mean sea level obtained by ROM and ECHAM5/MPIOM is shown in Fig. 12. The finer resolved ocean model is capable of reproducing some important features that are missing in the coarser ECHAM5/MPIOM version, e.g., the better representation of the Gulf Stream separation and the Labrador Current. In ECHAM5/MPIOM simulation (Fig.12 b) there is an unrealistic south-eastward extension of Subpolar Gyre (SPG). This feature can be explained by the coarser resolution of the ocean grid, and consequent “late” separation of the Gulf Stream causing the “blocking” of the Labrador Current, which leads to the eastward spread of the Labrador Sea water. Comparing NCEP and ECHAM5/MPIOM forced runs (Fig.12 c,d and Fig.13 a,b) an overestimation of the Labrador

Current is also seen in the second case (Fig. 12 d and Fig.13 b). This overestimation could be due to the fact that ECHAM5 forced run provides stronger outflow from the Arctic (Fig. 13 b). Additionally, the ECHAM5/MPIOM atmospheric forcing leads to a larger amount of sea ice in the Arctic (see below) and enhanced fresh water cycle in the high latitudes. Both these features increase Arctic freshwater export and its consequent accumulation in the SPG. The main difference in ROM-ECHAM5 compared to ECHAM5/MPIOM is that the Labrador Sea water released from the SPG is not blocked by the "late separated" Gulf Stream, and can flow along the North American coast. Despite this improvement, an unrealistic southward extension of the SPG and consequent overestimated zonality of the North Atlantic current is found in all the simulations.

We hypothesize the following explanation: in observations, the Labrador Sea water is sinking and flowing as upper deep water or intermediate water southward. Additionally, the Labrador Current, consisting of the fresh and cold surface water of the Labrador Sea, flows southward along the coast. In this case, a stronger North Atlantic current tends to reduce the Labrador Current coming from the opposite direction. In our simulations, the southward Labrador outflow in ROM-ECHAM5 is stronger than in ROM-NCEP due to more intense SPG, thus tending to "force" the North Atlantic current southward and Gulf Stream eastward. As different atmospheric data was used to force the same ocean model, we conclude that the overestimated eastward shift of the Gulf Stream, as well as the excessive zonality of the North Atlantic current in ROM-ECHAM5, are caused by biases in the atmospheric forcing (section 4.1.).

Atlantic meridional overturning circulation (AMOC) in ROM-ECHAM5 and ROM-NCEP differs significantly both in intensity and the vertical structure (Fig.14). The maximum of AMOC simulated by ROM-ECHAM5 reaches ca. 20 Sv, whereas in ROM-NCEP it is about 18 Sv, which seems to be more realistic. A value of approx. 18.5 Sv has been estimated from the RAPID array [Cunningham et al. 2007]. The reason for the overestimated AMOC in

ROM-ECHAM5 can be due to the enhanced deep water convection in the Labrador Sea and stronger SPG. In terms of vertical structure, the Antarctic bottom water (AABW) cell in ROM-ECHAM5 is strongly reduced in comparison with ROM-NCEP results (Fig. 14).

The ocean tidal forcing was derived from the full ephemeridic luni-solar tidal potential [Thomas et al., 2001]. For validation purposes, a least square harmonic analysis of sea level was performed. The ability of the model to simulate tidal dynamics is shown in Fig. 15. Here, we present only the M_2 constituent, which is the dominant component in the domain of our interest. In the eastern part of the North Atlantic the agreement between the model and observation is reasonable for a climate model. The amphidromic points are well captured, especially in the Greenland, Iceland, Norwegian (GIN) seas and North sea. In the western part of the North Atlantic, the disagreement between the model and observation is much larger. The tidal amplitude is strongly overestimated in the Labrador Sea, leading to the eastward shift of North Atlantic amphidromic point and underestimated along the US coast. The higher tidal amplitude in the Labrador Sea could be explained by reduced tidal energy transfer through the Hudson Strait into the Hudson Bay, where the amplitude is strongly underestimated. This reduction leads to the 'accumulation' of tidal energy in the Labrador Sea, which results in the increase of the amplitude.

In our region of interest, in particular at the North European shelves, ocean tidal dynamics plays an important role. Its influence on the climate was investigated by Müller et al. [2010]. Using the global coupled atmosphere – ocean general circulation model (AOGCM) ECHAM5/MPIOM they showed significant changes in the North Atlantic circulation caused by the induced tidal mixing and nonlinear interactions of tides with low frequency motion. Comparing two sets of our simulations (with and without tidal forcing) we also found some pronounced differences in the spatial structure of the circulation "ring": Gulf Stream – North Atlantic current – SPG – Labrador Current – Gulf Stream. Tidal stress interaction with irregular bottom topography generates an additional eddy field, whose energy is partly

transferred to the mean field in form of a basin scale steady cyclonic circulation. This effect is known as Neptune [Holloway, 1987, 1992] and induces changes in the barotropic streamfunction of the North Atlantic as compared to the non-tidal simulations. These changes cause a further southward penetration of the Labrador Current, which "pushes" the Gulf Stream southeastward. Evidence supporting this conclusion is presented in Figs. 15c and 15d, showing the concentrations in the upper 200 m of a numerical tracer whose concentration is kept constant and equal to unity south of 23ºN and with a half-time decay of 30 years. The plots show the mean tracer concentration and its relative difference from non-tidal run in the years 1980-1999, starting the simulations with and without tides from the same tracer concentration field in the year 1920. Figure 15c shows the concentration of the numerical tropical tracer in the tidal simulations, identifying the presence of waters of tropical origin,. As expected, a steep front in tracer concentration separates the tropical Gulf Stream from the Arctic Labrador Current. Figure 15d depicts the relative difference between the tropical tracer concentration distribution with and without tides. There is a remarkable reduction in the tropical tracer concentration (10-20%) along the North-American east coast down to Cape Hatteras, clearly pointing out a better representation of the Gulf Stream separation because the Labrador Current waters penetrate further south due to the inclusion of tides. The consequent shift of the North Atlantic current and the tidal circulation around the North Atlantic amphidromy supply more salty Atlantic water into the SPG, thus increasing its strength and convection activity in the Labrador Sea.

Additionally, our experiments show some tidal impact on the modelled climate over Europe (Fig.15e,f). Its influence on the Western European temperature can be clearly explained by the increased mixing. Still, there are large spatial variations. The winter and spring mean 1980-1999 2m temperature is 0.2-0.4K warmer, whereas in summer and autumn it is 0.2-0.4K colder.

The biases in ocean circulation described above are clearly reflected in the biases of SST and SSS (Figs. 16-17). Strong cold SST bias (up to 4 K) in ROM-ECHAM5 between 40°W and 60°W can be explained by the shift of the North Atlantic current in this simulation. An absence of this bias in ROM-NCEP (Fig. 16b) indicates that its origin comes from the ECHAM5/MPIOM atmospheric forcing (Fig. 16d). The negative salinity bias in the ROM-ECHAM5 results (Fig. 17c) shows a similar structure compared to the SST bias, indicating the overestimated southward propagation of the fresher Labrador Sea water (Fig. 12d and Fig.13b). Figures 17e and 17f show that the above mentioned negative SSS bias is not caused by the freshwater flux correction, but mainly connected with overestimated Labrador Sea water inflow in this region. First, the freshwater correction in the Labrador Sea is negligible compared to the natural freshwater input (Fig.17e,f). Second, the location of described bias salinity restoring tries to make the water saltier, but is too weak to eliminate the bias.

Another cold SST bias simulated by ROM forced by both ECHAM5/MPIOM and NCEP atmospheres occurs in the Norwegian Sea (Fig. 16). A possible explanation is the reduced oceanic heat transport into Norwegian Sea due to the excessive zonality of the North Atlantic current. On the other hand, there is a strong difference in SST bias between ROM-ECHAM5 (strong cold-bias) and ECHAM5/MPIOM (strong warm-bias) in GIN seas. This difference can be explained by the difference in ocean models resolution. Whereas ROM-MPIOM permits mesoscale eddies development and meandering of the North Atlantic Current (NAC), the coarsely resolved ECHAM5/MPIOM does not properly represent these features, leading to the advection of almost all of the warm NAC waters into the Arctic (Fig. 13 b,c).

The cold bias in ROM-ECHAM5 is also consistent with positive GIN seas sea ice extent anomalies. In our simulation, years with anomalously high sea ice extent in the GIN seas coincide with anomalously low SST in North and Baltic seas (Fig.18a). Simultaneously, the 2m temperature is anomalously low over the GIN seas, Barents Sea, parts of the Arctic Ocean and Northern and Central Europe (Fig.18b,c).

The simulated climatological sea surface temperature in the North Sea and the western part of the Baltic Sea is in a good agreement with observational climatologies (Fig.16). In the eastern part of the Baltic Sea, i.e. Gulf of Bothnia and Gulf of Finland, SST is underestimated by about 2K for ROM-ECHAM5. This is mainly caused by a cold bias in the atmospheric model in this region (Fig. 16d), which is subject of further investigations. The largest disagreement of sea surface salinity on the North European shelves with observational data occurs around Denmark, in the Gulf of Finland and at the Norwegian coast (Fig. 17). Both the vertical and the horizontal resolutions of the ocean model are not sufficient for a realistic representation of the physical processes in these regions. Note that both in the North and Baltic seas the fresh water correction in our simulations was completely switched off (see section 3). The strong model bias in the Wadden Sea is a consequence of the coarse vertical resolution. The dipole structure of salinity bias along the Norwegian coast is caused by relatively "smooth" modeled Baltic water outflow. The strong observed meandering of this outflow [Johannessen et al., 1989] and a consequent increased horizontal mixing with North Sea water is not resolved in our MPIOM setup.

One of the most complicated tasks in the modeling of the water circulation in the Baltic and the North seas is the representation of their exchange through the Danish straits. We realize that a vertical resolution of ca. 10 m and a horizontal resolution of ca. 10 km are not sufficient to reproduce exactly the high-frequency dynamics, associated with the pulse-like Baltic – North Sea water exchange through the small straits. Nevertheless, the modeled salinity of the Baltic Sea is in relatively good agreement with the observational data. As we do not use any kind of fresh water flux correction or salinity restoring in this region, this indicates that the total exchange was in balance with precipitation and river runoff into the Baltic Sea.

Sea ice thickness is presented in Fig. 19. The simulations are compared against the PIOMAS Arctic Sea Ice Volume Reanalysis data [Zhang and Rothrock 2003, Schweiger et al.

2011]. The results of ROM-ECHAM5 simulations show an overestimation of the Arctic sea ice extent as well as an overestimation of the ice thickness in the Central Arctic and East Siberian Sea. The last fact can be explained by the bias of MSLP of Aleutian Low in ECHAM5 [e.g. Roeckner et al. 2006] and consequent reduction of atmospheric heat transport from the Pacific Ocean. The NCEP forced simulations provide more realistic sea ice distribution in Arctic, indicating that the sea ice thickness overestimation in ROM-ECHAM5 is mainly caused by the atmospheric forcing. This fact is clearly demonstrated by the results obtained from the ECHAM5/MPIOM simulations (Fig. 19 d,h) where the ice thickness is overestimated by a factor of two in many parts of the Russian Arctic.

4.4 Ocean biogeochemistry

We now compare the simulated distributions of dissolved nutrients, i.e. PO_4^{3-} and NO_3^- to observations from the World Ocean Atlas [WOA, Garcia et al., 2010]. The model reproduces the low concentrations within the oligotrophic subtropical gyre and the higher concentrations in the Atlantic north of 40°N (Fig. 20). The latter results from reduced biological consumption during winter, when phytoplankton growth is limited by solar radiation and from upward mixing of nutrients during deep winter mixing. The locally enhanced phosphate concentration near the coast of NW Africa is also reproduced. The NCEP forced simulation achieves a better result, properly representing the phosphate maximum located around Cape Blanc, while ROM-ECHAM5 extends that maximum further north along the African coast. In this region, the modelled concentrations are clearly too high which is probably linked to a too strong upwelling of nutrients in this area. In the Northeast Atlantic, concentrations are likewise overestimated in both the ROM-NCEP and ROM-ECHAM5 simulations..

The modelled annual mean primary production shows the well-known pattern seen in observations and other models (Fig. 21). Low production is found within the vast subtropical gyres. High productivity is detected at high latitudes and along the tropical divergence zones

in the Pacific and the Atlantic. Moreover, the high productivity associated with coastal upwelling zones like e.g. along the western coast of Africa is reproduced. As it is known from previous studies [Steinacher et al., 2010], HAMOCC tends to overestimate production in the tropics and to underestimate it in the North Atlantic.

The vertical structure of nutrient distributions is shown in Fig. 22. The northern North Atlantic is characterized by overall low nutrient concentration through the water column. Here, nutrient depleted waters from the euphotic zone, where vigorous consumption by phytoplankton growth takes place, are transported downwards by strong vertical mixing and deep convection during winter. These waters are transported via the North Atlantic Deep Water further south at depths between 2000 m and 4000 m [Maier Reimer, 1993, Ilyina et al., 2013].

Well recognized in the model simulation are also the nutrient depleted subtropical gyres which extend down to a depth of approximately 800 m due to strong wind driven Ekman pumping (Fig.22a,b). The latter process is clearly underestimated in the NCEP forced simulation (Fig. 22c,d), as the vertical extension of the Ekman cells is clearly too shallow compared to the observations and the ECHAM forced simulation (Fig.22e,f). The highest nutrient concentrations are associated with Antarctic Intermediate Water at depths between 500 and 200 m. This water gains nutrients by remineralization of dead phytoplankton and zooplankton.

Integrated key parameters of the global carbon cycle compare well with values derived from the literature (Table 1). The globally integrated primary production lies in the upper range of published values while the globally integrated carbon uptake is in the lower range.

One of the greatest challenges in global biogeochemical modelling is the simulation of primary production (PP). Observational evidence is available mostly from satellites and is subject to large uncertainties. Global PP estimates from the twenty-four ocean colour-based models range over a factor of two (values from less than 40 PgC/yr to more than 60 PgC/yr,

[Carr et al., 2006]). The differences between different ocean-biogeochemistry models are in the same order of magnitude [Steinacher et al., 2010]. However, a high temporal correlation is identified between the ocean colour based estimated with both models, indicating that the internal variability in satellite based estimates is reliable [Carr et al., 2006]. Fig. 23 shows the correlation between primary production estimates of SeaWifs [Behrenfeld et al., 2006; Behrenfeld and Falkowski, 1997] and the ROM-NCEP simulation. At high latitudes, the relatively high positive correlation indicates the model's ability to reproduce the seasonal cycle of production, which relates on the limitation of the growing season due to temperature and light availability. Further south, in the realm of oligotrophic subtropical gyres, the nutrient availability becomes the dominating factor, which is mainly controlled by direct meteorological forcing (e.g. wind driven mixing, temperature, cloudiness). The complex interplay between these processes is less well captured by the model, and the correlation with satellite-based estimates is lower (in particular south of 20°N). However, as these regions suffer from general nutrient deficiency, primary production is lowest there.

Figure 23b shows the calendar month with highest primary production. In the central and eastern Atlantic north of 50°N, the main bloom generally occurs later with increasing latitude, mainly due to a shortening and later onset of the warm season. However, the large-scale circulation cannot be neglected. Whereas the southward advection of cooler water masses via the East Greenland current clearly postpones the spring bloom, the advection of warm waters at the eastern boundary via the North Atlantic drift and the Norwegian Current tends to have the opposite effect. This leads to a large difference between the western and eastern North Atlantic in terms of the timing of the main spring bloom (more than one month). The overall high correlation north of 50°N indicates that these processes are realistically captured by the model dynamics.

Pronounced meridional gradients between 30°N and 50°N along the 40°W indicate strong shifts in the timing of the production cycle on relatively small spatial scales (Fig. 23). In the

western part, the contributions of the cold Labrador outflow waters together with the warm and nutrient poor waters originating from the south leads to strong gradients in temperature and nutrient concentration. Fig. 23 shows generally high correlation with satellite based estimation along this section, which indicates that the main processes of nutrient cycling and productivity are well reproduced in this area. More important, is the actual export production which determines the carbon uptake. Here, the modelled export production lies well in the range of other published models (Table 1).

We have shown so far that the seasonal cycle of productivity is fairly well reproduced by the model. On the other hand, the interannual variability is of much lower amplitude than the seasonal cycle. Thus, a realistic estimation of interannual productivity variations in models must be considered as one of the most challenging issues of current global biogeochemical modeling efforts. Hence, the standard deviation of the monthly mean production is 10 to 15 times higher in our model than the standard deviation of yearly mean production in the North Atlantic. As free running coupled climate model simulations for the historical period cannot be directly compared to observations on a year to year basis, we use the NCEP reanalysis forced simulation for this purpose.

Fig. 24 clearly shows that the model has overall low predictive skills for annual mean variability. However, there is some significant predictive skill for interannual variations in March productivity. In order to explain the mismatch, both deficiencies in the model and in the satellite or color based model have to be discussed. On the one hand satellite based estimations are subject to several uncertainties related to both input variables to the ocean color model (like chlorophyl-a, SST etc.) and deficiencies in the ocean color model itself [Behrenfeldt and Falkowski, 1997; Carr et al., 2006; Saba et al., 2011]. On the other hand, the ROM-NCEP model deficiencies result from deficiencies in physical parameters and the circulation regime as well as deficiencies in the biogeochemical processes represented by HAMOCC. The latter constrains productivity to the presence of light and availability of

nutrients. After the spring bloom, nutrient supply is the dominating factor during most of the year. Its variability is subject to smaller scale physical processes like mesoscale eddies (which are not resolved in the model) and wind induced mixing. The interplay of all these processes is difficult to model, but determines the nutrient supply to the euphotic zone and thus productivity. Therefore, high predictive skills cannot be expected especially in a free evolving model where ocean and atmosphere are interactively coupled and thus lack any observational/reanalysis constrain. In addition to these physical limitations, the representation of biological processes further limits the predictive skill of the model (e.g. parameterization of the microbial loop, zooplankton grazing etc.).

Given the above, only few attempts have been undertaken so far to directly correlate productivity inferred from satellites with GCM based estimates. Steinacher et al. [2010], Seferian et al. [2012] and Henson et al. [2013] restricted their investigation to spatial correlations of long-term averages, and found only weak correlations between SeaWifs productivity and four different ocean biogeochemistry GCMs. Patali et al. [2013] used ocean color data only for a visual comparison of the large-scale pattern in the North Pacific. Henson et al. [2013] provide a temporal correlation between ocean color products and modeled productivity, but restricted this to the long-term mean seasonal cycle.

Still, we found some predictive skill with respect to interannual variations of March (Fig. 24b) and April productivity (not shown). During spring, nutrient saturated near-surface waters favor the onset of the spring bloom when light becomes available again. In this situation all the small-scale physical constraints on upward mixing of nutrients play only a minor role. Thus warming of the surface water together with increasing solar radiation determines the onset and strength of the spring bloom. These two processes are strongly related to the large-scale meteorological forcing. Specifically in the North Atlantic they are closely linked to the North Atlantic Oscillation [e.g., Hurrel and Deser 2009]. This large-scale mode of

atmospheric circulation is generally well captured in GCMs and most likely explains the good model skill in spring.

Although the focus of this paper is mainly on the North Atlantic, the model may potentially add value for the simulation of the complex shelf environment, which has been proposed to play an important role for the global carbon cycle via carbon shelf pumping [e.g., Tsunogai et al. 1999]. To assess the model predictive skill in shelf regions we investigate the nutrient cycle of the North Sea as part of the NW European shelf. The North Sea is a vast shelf sea composed of a well-mixed shallow southern part influenced by anthropogenic nutrient input and a deeper northern part which is seasonally stratified with a broad connection to the North Atlantic that supplies nutrients as well, e.g. Holt et al., [2012], Gröger et al., [2013]. The North Sea is a well-studied area (see Emeis et al., [2014] for an overview), with plenty of observations available for temperature, salinity and nutrients. The shelf dynamics is more complex compared to the open ocean. The biological turnover is often higher and the complex interplay between riverine nutrient input, vertical mixing, nutrient recycling and zooplankton leads to a complex and spatially varying pattern of the seasonal nutrient cycle, especially in the southern North Sea [e.g., Joint and Pomry, 1993].

We now aim to assess the model performance of the historical (ROM-ECHAM5) and NCEP (ROM-NCEP) simulation. Moreover, we investigate if there is an added value of the downscaling/regionalization. Unfortunately, the ECHAM5/MPIOM original runs were carried out without biogeochemistry, so that we have to employ the more recent run taken from the ECHAM6/MPIOM set-up employed for the CMIP5 ensemble [Ilyina et al., 2013].

Since ocean color based productivity estimates have been suspected to be valid for shallow (>250 m) and highly turbid regions [Saba et al., 2011], we use long-term nutrient observations from the Federal Maritime and Hydrographic Agency, Hamburg, Germany. Following the approach undertaken by Gröger et al. [2013], we assess how well the complex nutrient cycling in the North Sea can be reproduced by the model and if there are improvements

compared to the global ECHAM6/MPIOM model. Figure 25 shows that the downscaled historical ROM-ECHAM5 and ROM-NCEP runs perform better compared to the global ECHAM6/MPIOM simulation. All model runs have biases but the downscaled runs have least RMS values (ROM-ECHAM5=6.05; ROM-NCEP=6.27; ECHAM6/MPIOM=8.83) which are in the range of internal natural variability as indicated by the standard deviation of observations (STD=8.25). While the seasonal cycle of the global ECHAM6/MPIOM is nearly completely unrelated to the observed cycle, the downscaled runs can explain at least around 45% of the natural variability. However, all models fail to capture the full range of natural variability as indicated by the too low standard deviation (Fig.25).

There are several reasons for the low performance in nutrient cycling of the ECHAM6/MPIOM model. NO_3 concentrations are clearly too low in the southern North Sea. In the downscaled simulations phosphate is the limiting nutrient for productivity, but persistent NO_3 input from rivers leads to high concentrations in the vicinity of the coasts. The phosphate limitation near the coasts is in good agreement with observational evidence [e.g. Skogen et al. 2004; van der Zee and Chou 2005]. The global model was driven with no additional riverine nutrient input. This explains the too low NO_3 concentrations. Furthermore, statistical comparison with salinity data from the World Ocean Atlas (2013) indicates that all models correlate quite well with the observation based climatology (Fig.25), but the ECHAM6/MPIOM model bias is twice as large as the one from downscaled simulations. The differences are concentrated mainly along the outflow path of water from the Baltic Sea, which is located east of the North Sea and connected to it via small straits. This outflow from the Baltic is clearly too fresh in the ECHAM6/MPIOM model, indicating problems in simulating realistically the water mass exchange (mainly related to its too coarse resolution). The properties of water masses have large influences for the phytoplankton dynamics along the coast of Norway. An important feature of the North Sea is the summer thermal stratification, which leads to a nutrient limitation of production in the upper water layers.

Fig.26 shows that the downscaled ROM-ECHAM5 model captures this feature very well, when in July and August a sharp thermocline develops at around 20 to 25 m depth. This thermocline is not well pronounced in the ECHAM6/MPIOM simulation pointing to an overestimation of vertical mixing in the water column.

A comprehensive validation of HAMOCCs global biogeochemical fields is available from Ilyina et al. [2013]. More detailed validation of model's biogeochemistry with particular focus on the North Sea is available from an uncoupled model version with a somewhat lower spatial resolution [Gröger et al., 2013].

5. Conclusions and discussion

A global ocean – sea ice – marine biogeochemistry coupled model (ROM) comprising the REgional atmosphere MOdel (REMO), the Max Planck Institute Ocean Model (MPIOM), the HAMburg Ocean Carbon Cycle (HAMOCC) model, and the Hydrological Discharge (HD) model was described and validated. All components are coupled via OASIS coupler. The regional coupled model ROM was validated against observational and reanalysis data. Historical simulations were performed using two different forcing data sets. The comparison between results obtained by ROM driven with reanalysis data (NCEP/NCAR) and with global AOGCM (ECHAM5/MPIOM) boundary conditions allowed an attribution of the sources of the model biases. For ROM-NCEP, they provide from ROM only, whereas for ROM-ECHAM5 they are additionally caused by the driving global model (ECHAM5/MPIOM) through the atmospheric boundary conditions and the ocean forcing outside the coupled area.

The ROM coupled system forced by the global AOGCM can improve the representation of key climatic variables on the regional scale by including physical processes into the MPIOM which are not accounted for in the driving model. These improvements are mainly visible in the ocean model results. For example, the consideration of ocean tides lead to a more realistic

Gulf Stream separation and an increase of the tropical water inflow into the SPG, enhancing the deep water convection in this region. Additional effect of the ocean tides on the climate is an increase of the ocean vertical mixing causing, for example, slightly warmer winter/spring (0.2K-0.4K) and slightly colder summer/autumn (-0.2K - -0.4K) in Western Europe.

In uncoupled RCMs, the added value is mainly caused by the better representation of orography. Dynamical downscaling from GCM may be considered as a kind of "intelligent interpolation" of atmospheric fields. Recent studies have shown that there are cases when regional atmosphere-ocean climate models (RAOCMs) are capable of improving the simulation of the climate system by the driving model, e.g. Li et al, [2012]. The comparison between the ROM-NCEP and ROM-ECHAM5 provided evidence that the added value of the downscaling approach varies with the season, the region, and the variable / model component which is analyzed (section 4). Promising results are found for example for precipitation (section 4.2.), which clearly document the added value of the present approach.

It is well known that biases in the driving GCM can seriously impede the potential of RCM to skillful simulations and that to a large extent RCMs reproduce the successes and failures of the global models used for driving them [e.g., Rummukainen, 2010], just in a higher resolution. However, the influence of the lateral boundary conditions on the RCM simulated climate depends on the relative importance of internal and external variability. It has been shown that the choice of domain size and location affects the balance between the boundary and internal model forcing in the simulations [e.g., Diaconescu et al, 2013]. Therefore, the large-scale atmospheric circulation may be modified in coupled RAOCMs. In ROM these changes can be even more pronounced because of the global ocean model set-up [e.g., Sein et al. 2014]. The differences in the modelled SPG may lead, for example, to differences in the cyclogenesis over the North Atlantic, and thus to changes in paths and intensity of extra-tropical cyclones over this area.

Added value of a different kind can be obtained by implementing a high-resolution ocean component for regions like the North and Baltic seas. In ECHAM5/MPIOM simulations the ocean model is not capable to represent the exchange through the Danish Straits because of the lack of the model resolution. It leads to freshening of the Baltic Sea and finally to zero salinity in the steady model state. This does not allow a correct simulation of salinity changes in the Baltic Sea for future climate conditions, with increase of the freshwater inflow into the Baltic Sea. In contrast, our ROM model is capable to simulate the exchange between both basins and provides realistic salinity for the Baltic Sea.

The model has proven its ability to sufficiently reproduce the main dynamics of biogeochemical tracers. The seasonal cycle of nutrients in the high latitudes compares well with observations. Furthermore the dynamics of primary production is reproduced well in the regions of coastal and equatorial upwelling as well as the strong seasonality of primary production in the high latitudes. Thus, the modelled globally integrated net primary production, the export production and the total ocean carbon uptake are well within the range of published values. Accordingly, the characteristic nutrient distribution within the different deep and intermediate water masses (e.g. nutrient poor NADW, and nutrient rich AAIW and AABW) compares well with observations.

The model also demonstrated improvements of shelf processes such as the seasonal thermal stratification and nutrient cycling in the North Sea on the NW European shelf. These processes are substantially better represented than in the global unstretched MPI-ESM CMIP5 model without downscaling. No improvements could be achieved with respect to reproducing interannual variations of yearly mean productivity in the North Atlantic. However, area averaged interannual variations of productivity for the North Atlantic (30°W-10°E; 30°S-65°N) are positively correlated to corresponding estimates from ocean color (r=0.49) and good skills could be achieved with respect to interannual variations in spring production.

These are related to the strength of the first production peak of the year and probably strongly tied to the North Atlantic Oscillation.

To our best understanding, the main disadvantages of the proposed model are related to the limitation of the vertical resolution, i.e. the upper ocean model layer has to be thick enough to handle the ocean tides and underwater part of the sea ice. Another disadvantage is that the bias and internal variability generated from the global domain can influence the result in the coupled domain, making it difficult to separate the sources of bias. The apparent disadvantages in the limitation of the horizontal resolution and computational time are questionable. The ocean component in our model allows the required refinement of the computational grid in the coupled domain, keeping there up to 70% of grid nodes. Still, it does not mean that the ocean resolution outside the coupled area is neglected. Even though the ocean model grid is coarser outside the regional atmosphere domain, it should be fine enough to reproduce general features of the global ocean circulation. This condition can also be considered as disadvantage, i.e. our ocean set-ups usually have larger amount of horizontal grid nodes than those in standard setups of limited area ocean model.

We conclude that the proposed model system improves many aspects of the regional climate, remarkably the ocean, while some biases persist in other model components. Therefore, there is still potential for improvement. ROM is a powerful model system that can be used to estimate possible impacts of climate change on the regional scale. In fact, the model has been developed to allow the investigation of processes in different regions of the globe (Fig.27). These include current model applications to study climate variability in the North Atlantic (Fig.27a), analyse the sensitivity of simulated regional climate to the choice of coupled domain in Arctic (Fig. 27b), simulate the South-East Asia climate and its future change with the focus on typhoons generated in this region (Fig. 27c), investigate the West African monsoons and hurricanes in Tropical Atlantic (Fig.27d) and study the Indian monsoon (Fig.27e). Further model applications allow improving the results of global climate

models as well as understanding of the impact of relatively small-scale atmospheric process (not resolved in global AOGCMs) on present and future climate.

Acknowledgements

The authors would like to gratefully thank Ernst Maier-Reimer whose sudden death prevented him from co-authoring this manuscript. Ernst contributed significantly to this work by giving technical advice and steering the scientific model development. The authors are also thankful for his valuable help with the interpretation of simulated results of the coupled model as long as it was possible for him.

The model simulations were performed at the German Climate Computing Center (DKRZ). We thank ECMWF (http://www.ecmwf.int) and NOAA (http://www.esrl.noaa.gov) for providing ERA-Interim and NCEP reanalysis data, Helmuth Haak for helping us with the MPIOM model and Marina Tarasova and Timothy Petliar for useful discussions. The work was supported by the German Federal Ministry of Education and Research (BMBF) under the projects NORDATLANTIK (research grant 03F044E), MiKlip-DEPARTURE (research grant 01LP1129C), MiKlip-PRODEF (research grant 01LP1120A) and SPACES-AGULHAS (research grant 03G0835B).

We thank the anonymous reviewers and the editor for the constructive suggestions and critical remarks, which helped to improve the manuscript.

References

Adam, J. C., and D. P. Lettenmaier (2003), Adjustment of global gridded precipitation for systematic bias, *J. Geophys. Res.*, *108*(D9), 4257, doi:10.1029/2002JD002499.

Arakawa A. and V. R. Lamb (1977), Computational design of the basic dynamical processes of the UCLA general circulation model, *Methods Comput. Phys*., *17*, 173-265.

Artale, V., S. Calmanti, A. Carillo, A. Dell'Aquila, M. Herrmann, G. Pisacane, P. M. Ruti, G. Sannino, M. V. Struglia, F. Giorgi, X. Bi, J. S. Pal, S. Rauscher (2009), An atmosphere ocean regional climate model for the Mediterranean area: assessment of a present climate simulation, *Clim. Dyn. 35*, 721-740

Avissar, R., and R. A. Pielke (1989), A parameterization of heterogeneous land surfaces for atmospheric numerical models and its impact on regional meteorology, *Monthly Weather Review*, *117*, 2113-2136.

Balmaseda M.A,. K. Mogensen, A. Weaver, (2013), Evaluation of the ECMWF Ocean Reanalysis ORAS4. *Q. J. R. Meteorol. Soc., 139,* 1132–1161, doi:10.1002/qj.2063

Behrenfeld, M. J. and P. G. Falkowski (1997), Photosynthetic rates derived from satellite-based chlorophyll concentration, *Limnol. Oceanogr., 42*, 1–20.

Behrenfeld, M. J., R. T. O'Malley, D. A. Siegel, C. R McClain, J. L. Sarmiento, G. C. Feldman, A. J. Milligan, P. G. Falkowski, R. M. Letelier, and E. S. Boss (2006), Climate-driven trends in contemporary ocean productivity, *Nature, 444*, 752–755.

Bougeault, P. (1983), A non-reflective upper boundary condition for limited-height hydrostatic models, *Monthly Weather Review*, *111*, 420-429.

Bülow, K. , C. Dietrich, A. Elizalde, M. Gröger, H. Heinrich, S. Hüttl-Kabos, B. Klein, B. Mayer, H. M. Meier, U. Mikolajewicz, N. Narayan, T. Pohlmann, G. Rosenhagen, S. Schimanke, D. Sein, and J. Su, J. (2014), Comparison of three regional coupled ocean atmosphere models for the North Sea under today's and future climate conditions, *KLIWAS-27/2014, Koblenz, BfG,* 265 p. doi:10.5675/Kliwas_27/2014

Carr, M.-E., et al. (2006), A comparison of global estimates of marine primary production from ocean color, *Deep-Sea Res. Pt. II, 53*, 741–770, doi:10.1016/j.dsr2.2006.01.028.

Carton J. A. and B. S. Giese, (2008), A reanalysis of ocean climate using Simple Ocean Data Assimilation (SODA), *Mon. Weather Rev., 136*, 2999-3017.

Charnock, H., (1955), Wind stress on a water surface, *Q.J.R. Meteorol. Soc. 81*, 639–640.

Chen, R., G. Flerl, and C. Wunsch, (2014), A description of local and nonlocal eddy-mean flow interaction in a global eddy-permitting state estimate. *J. Phys. Oceanogr.*, 44, 2336-2352.

Cunningham, S. A., T. Kanzow, D. Rayner, M. O. Baringer, W. E. Johns, J. Marotzke, H. R. Longworth, E. M. Grant, J. J.-M. Hirschi, L. M. Beal, C. S. Meinen, H. L. Bryden, (2007), Temporal variability of the Atlantic meridional overturning circulation at 26.5 degrees N, *Science, 317*(5840), 935-938. 10.1126/science.1141304

Davies H.C. (1976), A lateral boundary formulation for multi-level prediction models, *Q. J. R. Meteorol. Soc. 102*, 405–418.

Dawe J.T. and L. Thompson (2006), Effect of ocean surface currents on wind stress, heat flux, and wind power input to the ocean, *Geophys. Res. Let., 33*, L09604, doi:10.1029/2006GL025784

Dee, D. P., et. al. (2011), The ERA-Interim reanalysis: configuration and performance of the data assimilation system, *Q.J.R. Meteorol. Soc., 137*, 553–597. doi: 10.1002/qj.828

Déqué, M. and J. P. Piedelievre (1995), Latest issue climate simulation over Europe, *Climate Dynamics, 11*, 321-339.

Déqué, M., D. P. Rowell, D. Lüthi, F. Giorgi, J. H. Christensen, B. Rockel, D. Jacob, E. Kjellström, M. de Castro, and B. van den Hurk (2007), An intercomparison of regional climate simulations for Europe: assessing uncertainties in model projections, *Climatic Change, 81*, 53-70. DOI: 10.1007/s10584-006-9228-x.

Diaconescu E.P., R. Laprise (2013), Can added value be expected in RCM-simulated large scales? *Clim. Dynam. 41*, 1769–1800, doi:10.1007/s00382-012-1649-9

Döscher R., U. Willen, C. Jones, A. Rutgersson, H. E. M. Meier, U. Hansson, L. P. Graham, (2002), The development of the regional coupled ocean-atmosphere model RCAO, *Boreal Env. Res., 7*, 183-192

Emeis, K.-C., et al., The North Sea - A shelf sea in the Anthropocene*, J. Mar. Syst.* (2014), http://dx.doi.org/10.1016

Feser, F., B. Rockel, H. von Storch, J. Winterfeldt, and M. Zahn (2011), Regional Climate Models add Value to Global Model Data: A Review and selected Examples, *Bulletin of the American Meteorological Society*, doi: 10.1175/2011BAMS3061.1.

Fouquart, Y., and B. Bonnel (1980), Computations of solar heating of the Earth's atmosphere: A new parameterization, *Beiträge zur Physik der Atmosphäre, 53*, 35-62.

Fuchs, T., U. Schneider, and B. Rudolf (2007), Global Precipitation Analysis Products of the GPCC, Global Precipitation Climatology Centre (GPCC), *Deutscher Wetterdienst,* Offenbach, Germany.

Garcia, H. E., R. A. Locarnini, T. P. Boyer, J. I. Antonov, M. M. Zweng, O. K. Baranova, and D. D. Johnson (2009), World ocean atlas 2009, Vol. 4, nutrients (phosphate, nitrate, silicate), edited by: Levitus, S., NOAA Atlas nesdis 71, us government printing office, Washington, DC, 398 pp., 2010.

Gent P. R., J. Willebrand, T. McDougall and J. C. McWilliams (1995), Parameterizing eddy-induced tracer transports in ocean circulation models, *J. Phys. Oceanogr.*, *25,* 463-474.

Granskog M., Kaartokallio H., Kuosa H., Thomas D. N. and Vainio J. (2006), Sea ice in the Baltic Sea - A review, *Est. Coast. Shelf Sci.,70,* 145-170.

Griffies S. M. (1998), The Gent - McWilliams skew flux, *J. Phys. Oceanogr*., *28*, 831-841.

Gröger, M., and U. Mikolajewicz, (2011), Note on the air-sea gas exchange at high temperatures, *Ocean Modelling*, doi:10.1016/j.ocemod.2011.05.003

Gröger M., E. Maier-Reimer, U. Mikolajewicz, A. Moll and D. Sein (2013), NW European shelf under climate warming: Implications for open ocean – shelf exchange, productivity, and carbon absorption, *Biogeosciences, 10*, 3767-3792, doi:10.5194/bg-10-3767-2013.

Gustafsson N., L. Nyberg, A. Omstedt (1998), Coupling of a high resolution atmospheric model and an ocean model for the Baltic Sea, *Mon Weather Rev. 126*: 2882–2846

Hagemann, S., and L. Dümenil, (1998), A parameterization of the lateral waterflow for the global scale, *Climate Dyn., 14*, 17-31.

Hagemann, S., and L. Dümenil Gates (2001), Validation of the hydrological cycle of ECMWF and NCEP reanalyses using the MPI hydrological discharge model, *J Geophys Res 106,* 1503-1510.

Hagemann, S., H. Göttel, D. Jacob, P. Lorenz and E. Roeckner (2009), Improved regional scale processes reflected in projected hydrological changes over large European catchments, *Climate Dyn. 32* (6), doi: 10.1007/s00382-008-0403-9: 767-781.

Heath, M. R., A. C. Edwards, J. Pätsch, W. R. Turell (2002), Modelling the behaviour of nutrients in the coastal waters of Scotland. Fisheries Research Services Marine Laboratory Aberdeen, Scottish Executive Central Research Unit Contract, 106 pp

Heinze, C., E. Maier-Reimer, A. M. E. Winguth, and D. Archer, (1999), A global oceanic sediment model for long term climate studies, *Global Biogeochem. Cycles, 13*, 221–250.

Henson, S., Cole ,H., Beaulieu,C., and Yool,A., (2013), The impact of global warming on seasonality of ocean primary production, *Biogeosciences, 10*, 4357–4369.

Hibler, W. D. (1979), A dynamic thermodynamic sea ice model. *J. Phys. Oceanogr.*, *9*, 815-846.

Holloway, G. (1987) Systematic forcing of large-scale geophysical flows by eddy-topography interaction. *J. Fluid Mech., 184,* 463-476.

Hollowaz, G. (1992) Representing topographic stress for large-scale ocean models, *J. Phys. Oceanogr., 22*, 1033-1046

Holt, J., Butenschon, M., Wakelin, S. L., Artioli, Y., Allen, J. I., (2012), Oceanic controls on the primary production of the northwest European continental shelf: model experiments under recent past conditions and a potential future scenario. *Biogeosciences 9*, 97-117.

Hoskins, B. J., and P. J. Valdes (1990), On the existence of storm-tracks. *J. Atmos. Sci., 47*, 1854–1864.

Hueging H, K. Born, R. Haas, D. Jacob, J. G. Pinto (2013), Regional changes in wind energy potential over Europe using regional climate model ensemble projections, *J. Appl. Meteor. Climatol., 52,* 903-917.

Hurrell, J. W., and C. Deser, (2009), North Atlantic climate variability: The role of the North Atlantic Oscillation. *J. Mar. Syst., 78*, 1, 28-41.

Ilyina, T., K. Six, J. Segschneider, E. Maier-Reimer, H. Li, and I. Nunez-Riboni (2013), The global ocean biogeochemistry model HAMOCC: model architecture and performance as component of the MPI-Earth system model in different CMIP5 experimental realizations, *J. Adv. Model. Earth Syst. 5*, doi10.1002/jame.200172013.

Jacob, D., (2001), A note to the simulation of the annual and interannual variability of the water budget over the Baltic Sea drainage basin, *Meteorology and Atmospheric Physics*, *77*(1-4), 61-73.

Jacob, D., et al., (2001), A comprehensive model intercomparison study investigating the water budget during the BALTEX-PIDCAP period. *Meteorology and Atmospheric Physics*, *77*(1-4), 19-43.

Johannessen J. A., O. M. Johannessen and P. Haugan (1989), Remote sensing and model simulation study in the Norwegian coastal current during the algal bloom in May 1988, *International Journal of Remote Sensing 10*(12), 1893-1906.

Joint, I., and A. Pomroy, (1993), Phytoplankton biomass and production in the southern North Sea. *Mar. Ecol. Prog. Ser., 99*, 169-182.

Jungclaus, J. H., N. Keenlyside, M. Botzet, H. Haak, J. -J. Luo, M. Latif, J. Marotzke, U. Mikolajewicz, E. Roeckner (2006), Ocean circulation and tropical variability in the coupled model ECHAM5/MPI-OM.J, *Climate, 19*, 3952–3972.

Jungclaus, J. H., N. Fischer, H. Haak, K. Lohmann, J. Marotzke, D. Matei, U. Mikolajewicz, D. Notz, and J. S. von Storch (2013), Characteristics of the ocean simulations in MPIOM, the ocean component of the MPI-Earth system model, *J. Adv. Model. Earth Syst., 5*, 422–446, doi:10.1002/jame.20023.

Kerr, R. A. (2013), Forecasting Regional Climate Change Flunks Its First Test, *Science, 339*, 638-638, doi:10.1126/science.339.6120.638

Klemp, J. B., and D. R. Durran (1983), An upper boundary condition permitting internal gravity wave radiation in numerical mesoscale models, *Monthly Weather Review*, *111*, 430-444.

Kistler, R., et al. (2001), The NCEP/NCAR 50 year reanalysis: monthly-means CD-ROM and documentation, *B. Am. Meteorol. Soc., 82*, 247–267

Laprise, R, R. de Elía, D. Caya, S. Biner, P. Lucas-Picher, E. P. Diaconescu, M. Leduc, A. Alexandru, L. Separovic, (2008), Challenging some tenets of Regional Climate Modelling. *Meteor Atmos Phys 100,* 3–22. Special Issue on Regional Climate Studies. doi:10.1007/s00703-008-0292-9

Legutke, S. and R. Voss (1999), The Hamburg Atmosphere-Ocean Coupled Circulation Model ECHO-G, *Tech. Rep. 18, Ger. Clim. Comput. Cent., Hamburg, Germany.*

Lehmann, A., P. Lorenz, and D. Jacob (2004), Modelling the exceptional Baltic Sea inflow events in 2002–2003*, Geophys. Res. Lett., 31*, L21308, doi:10.1029/2004GL020830.

Le Querer et al. (2009), Trends in the sources and sinks of carbon dioxide, *Nat. Geosci., 2*, 831 –836, doi: 10.1038/ngeo689

Levitus, S., T .P. Boyer, M. E. Conkright., T. O'Brien., J. Antonov, C. Stephens, L. Stathoplos, D. Johnson, and R. Gelfeld (1998), World Ocean Database 1998: Volume 1:

Introduction, NOAA Atlas NESDIS 18, Ocean Climate Laboratory, National Oceanographic Data Center, U.S. Gov. Printing Office, Wash., D.C.

Li, T., G. Q. Zhou (2010), Preliminary results of a regional air-sea coupled model over East Asia, *Chin. Sci. Bull*, *55,* 2295–2305

Li, H., M. Kanamitsu, and S.-Y. Hong (2012), California reanalysis downscaling at 10 km using an ocean-atmosphere coupled regional model system, *J. Geophys. Res.*, *117*, D12118, doi:10.1029/2011JD017372

Lorkowski, I., J. Paetsch, A. Moll, and W. Kühn (2012),: Interannual variability of carbon fluxes in the North Sea from 1970 to 2006 – comparing effects of abiotic and biotic drivers of the gas-exchange of CO2, *Esutar. Coast. Shelf S.*, *100*, 38–57.

Maier-Reimer, E., I. Kriest, J. Segschneider, and P. Wetzel (2005), Technical description of the HAMburg Ocean Carbon Cycle model, version 5.1 (HAMOCC5.1), and of its interface to MPIOM, available at: http://edoc.mpg.de/get.epl?fid=17575&did=249293&ver=0.

Maier-Reimer, E (1993), Geochemical cycles in an ocean general circulation model: Preindurstrial tracer distributions. *Global Biogeochemical cycles*, *7,* 645—677.

Majewski, D. (1991), The Europa Modell of the Deutscher Wetterdienst. *Seminar Proceedings ECMWF*, ECMWF, Shinfield Park, Reading, Berks, United Kingdom, *2*, 147-191.

Marsland, S. J., H Haak, J. H. Jungclaus, M. Latif and F. Roeske, (2002), The Max-Planck-Institute global ocean/sea ice model with orthogonal curvilinear coordinates, *Ocean Modelling*, *5* (2), 91-126.

Metzger, E. J., O. M. Smedstad, P. G. Thoppil, H. E. Hurlburt, J. A. Cummings, A. J. Wallcraft, L. Zamudio, D. S. Franklin, P. G. Posey M. W. Phelps, P. J. Hogan, F. L. Bub and C. J. Dehaan, (2014) US Navy Operational Global Ocean and Arctic Ice Prediction Systems. *Oceanography,* 27, 3, doi:10.5670/oceanog.2014.66

Meybeck, M., and A. Ragu (1995), The Annotated Digital Atlas of Global water Quality, available under: http://www.gemswater.org/atlas-gwq/intro-e.html

Meybeck M, A. Ragu, (1997), River discharges to the oceans: an assessment of suspended solids, major ions and nutrients. GEMS/EAP Report.

Mikolajewicz., U., D. Sein, D. Jacob, T. Kahl, R. Podzun, T. Semmler (2005), Simulating Arctic sea ice variability with a coupled regional atmosphere-ocean-sea ice model. Meteorologische Zeitschrift, *14* (6), 793-800.

Morcrette, J.-J., and Y. Fouquart (1986), Pressure and temperature dependence of the absorption in longwave radiation parameterizations. *Beiträge zur Physik der Atmosphäre*, *59*, 455-469.

Müller, M., H. Haak, J. H. Jungclaus, J. Sündermann, M. Thomas (2010), The effect of ocean tides on a climate model simulation. Ocean Modelling *35*, 304–313

Nicholls, J, and R. Toumi, (2013), On the lake effects of the Caspian Sea. *Q. J. R. Meteorol. Soc.* doi: 10.1002/qj.2222

Nordeng, T. E. (1994), Extended versions of the convection parametrization scheme at ECMWF and their impact upon the mean climate and transient activity of the model in the tropics. *Research Department Technical Memorandum No. 206*, ECMWF, Shinfield Park, Reading, Berks, United Kingdom.

Orr, J., E. Maier-Reimer, U. Mikolajewicz, P. Monfray, J. L. Sarmiento, J. R. Toggweiler, N. K. Taylor, J. Palmer, N. Gruber, C.-L. Sabine, C. le Quere, R. M. Key, and J. Boutin (2001), Estimates of anthropogenic carbon uptake from four 3-d global ocean models, *Global Biogeochem. Cycles, 15*, 43–60.

Patara, L., M. Vichi, S. Simona Masina, (2012), Impacts of natural and anthropogenic climate variations on North Pacific plankton in an Earth System Model. *Ecological Modelling 244*, 132– 147

Pätsch, J. and H.-J. Lenhart (2004), Daily loads of nutrients, total alkalinity, dissolved inorganic carbon and dissolved organic carbon of the european continental rivers for the years 1977–2002, reports center for marine und climate research – Series b: Oceanography 2004, University of Hamburg.

Pätsch, J. and W. Kühn (2008), Nitrogen and carbon cycling in the North Sea and exchange with the North Atlantic - a model study, Part I. Nitrogen budget and fluxes. *Continental Shelf Research, 28*, 767-787.

Pinto, J. G., U. Ulbrich, G. C. Leckebusch, T. Spangehl, M. Reyers, S. Zacharias (2007), Changes in storm track and cyclone activity in three SRES ensemble experiments with the ECHAM5/MPIOM1 GCM. *Clim. Dyn. 29*, 195–210.

Pullen J., J. D. Doyle, R. P. Signell (2006), Two-way air-sea coupling: A study of the Adriatic. *Mon Weather Rev, 134*, 1465–1483.

Ratnam, J. V., F. Giorgi, A. Kaginalkar, S. Cozzini (2008), Simulation of the Indian monsoon using the RegCM3-ROMS regional coupled model. *Clim. Dyn*. *33*, 119-139.

Rechid, D. and D. Jacob, (2006), Influence of monthly varying vegetation on the simulated climate in Europe. *Meteorologische Zeitschrift, 15*, 99-116.

Rinke, A., R. Gerdes, K. Dethloff, T. Kandlbinder, M. Karcher, F. Kauker, S. Frickenhaus, C. Köberle and W. Hiller (2003), A case study of the anomalous Arctic sea ice conditions during 1990: insight from coupled and uncoupled regional climate model simulations. *J. of Geophys. Res., 108* (D9), 4275, doi:10.1029/2002JD003146

Roeckner, E., K. Arpe, L. Bengtsson, M. Christoph, M. Claussen, L. Dümenil, M. Esch, M. Giorgetta, U. Schlese, and U. Schulzweida (1996), The Atmospheric General Circulation Model ECHAM-4: Model Description and Simulation of Present-Day-Climate. *MPI für Meteorologie, Report 218.*

Roeckner, E., G. Bäuml, L. Bonaventura, R. Brokopf, M. Esch, M. Giorgetta, S. Hagemann, I. Kirchner, L. Kornblueh, E. Manzini, A. Rhodin, U. Schlese, U. Schulzweida, and

A. Tompkins (2003), The atmospheric general circulation model ECHAM 5. PART I: Model description. *MPI für Meteorologie, Report 349*

Roeckner E, R. Brokopf, M. Esch, M. Giorgetta, S. Hagemann, L. Kornblueh, E. Manzini, U. Schlese, U. Schulzweida (2006), Sensitivity of simulated climate to horizontal and vertical resolution in the ECHAM5 atmosphere model. *J. Clim., 19*, 3771–3791.

Roeske, F. (2001), An atlas of surface fluxes based on the ECMWF re-analysis – a climatological dataset to force global ocean general circulation models. *MPI für Meteorologie, Report 323*, 31pp.

Rudolf, B., and F. Rubel (2005), Global precipitation. In: Hantel. M. (ed) Observed global climate, Chap. 11. Landolt–Boernstein: numerical data and functional relationships in science and technology – new series, Group 5: Geophysics, vol. 6, Springer, Berlin Heidelberg New York, p 567.

Rummukainen, M. (2010), State-of-the-art with regional climate models, *Clim. Change*, *1*, 1, 82–96.

Saba, V. S., M. A. M. Friedrichs, D. Antoine, R. A. Armstrong, I. Asanuma, M. J. Behrenfeld, A. M. Ciotti, M. Dowell, N. Hoepffner, K. J. W. Hyde, J. Ishizaka, T. Kameda, J. Marra, F. Melin, A. Morel, J. O'Reilly, M. Scardi, W. O. Smith, T. J. Smyth, S. Tang, J. Uitz, K. Waters, and T. K. Westberry, (2011), An evaluation of ocean color model estimates of marine primary productivity in coastal and pelagic regions across the globe. *Biogeosciences 8*, 489–503.

Sanna, A., P. Lionello, and S. Gualdi (2013), Coupled atmosphere ocean climate model simulations in the Mediterranean region: effect of a high-resolution marine model on cyclones and precipitation. *Nat. Hazards Earth Syst. Sci*., *13*, 1567-1577, doi:10.5194/nhess-13-1567-2013.

Schaeffer P., Y. Faugere, J. F. Legeais, A. Ollivier, T. Guinle, N. Picot (2012), The CNES CLS11 Global Mean Sea Surface Computed from 16 Years of Satellite Altimeter Data. *Marine Geodesy, Special Issue, Jason-2, .35*.

Schweiger, A., R. Lindsay, J. Zhang, M. Steele, H. Stern (2011), Uncertainty in modeled arctic sea ice volume, *J. Geophys. Res.*, doi:10.1029/2011JC007084

She, J., P. Berg, J. Berg, (2007), Bathymetry impacts on water exchange modelling through the Danish Straits. *J. of Marine Systems, 65*, 450–459

Seferian, R., L. Bopp, M. Gehlen, J. Orr, J., C. Ethe, P. Cadule, O. Aumont, D. Salas-y-Melia, A. Voldoire, and G. Madec (2012), Skill assessment of three Earth system models with common marine biogeochemistry, *Clim. Dyn*. doi:10.1007/s00382-012-1362-8, 2012.

Sein, D. V., N. V. Koldunov, J. G. Pinto, W. Cabos, (2014), Sensitivity of simulated regional Arctic climate to the choice of coupled model domain. *Tellus A*, *66,* 23966 doi:10.3402/tellusa.v66.23966.

Semmler, T., D. Jacob, K. H. Schlünzen, R. Podzun, (2002), Influence of sea ice treatment in a regional climate model on boundary layer values in the Fram Strait region. *Monthly Weather Review*, *132*, 985–999.

Seo H, A. J. Miller, J. O. Roads, (2007) The scripps coupled ocean-atmosphere regional (SCOAR) model with applications in the Eastern Pacific sector. *J Clim, 20,* 381–402

Simmons, A. J., and D. M. Burridge (1981), An energy and angular-momentum conserving vertical finite-difference scheme and hybride vertical coordinate. *Monthly Weather Review*, *109*, 758-766.

Skogen, M. D., H. Søiland, and E. Svendsen, (2004), Effects of changing nutrient loads to the North Sea, *J. Mar. Sys., 46*, 23–38

Somot, S., F. Sevault, M. Déqué, (2006), Transient climate change scenario simulation of the Mediterranean Sea for the 21st century using a high-resolution ocean circulation model. *Clim. Dyn*. *27*, 851-879.

Somot, S., F. Sevault, M. Déqué, M. Crépon, (2008), 21st Century climate change scenario for the Mediterranean using a coupled atmosphere- ocean regional climate model. *Glob. Planet Change 63*, 112-126.

Stacke, T. and S. Hagemann (2012), Development and validation of a global dynamical wetlands extent scheme. *Hydrol. Earth Syst. Sci. 16*, doi:10.5194/hess-16-2915-2012: 2915-2933

Steele, M., R. Morley, and W. Ermold (2001), PHC: A global ocean hydrography with a high quality Arctic Ocean, *J. Climate, 14*, 2079-2087.

Steinacher, M., F. Joos, T. L. Frölicher, L. Bopp, P. Cadule, V. Cocco, S. C. Doney, M. Gehlen, K. Lindsay, J. K. Moore, B. Schneider, and J. Segschneider (2010), Projected 21st century decrease in marine productivity: a multi-model analysis. *Biogeosciences*, *7*, 979–1005, doi10.5194/bg-7-979-2010.

Stössel A. (1992), The Hamburg sea-ice model. *Tech. Rep. 3, Ger. Clim. Comput. Cent., Hamburg, Germany.*

Su, J., D. V. Sein, M. Mathias, B. Mayer, K. O'Driscoll, X. Chen, U. Mikolajewicz, T. Pohlmann (2014), Marine downscaling the global hindcast to the North Sea: a comparison of a global and a regional ocean model simulations. *Tellus A, 66*, 23927, http://dx.doi.org/10.3402/tellusa.v66.23927

Taylor K. E., R. J. Stouffer, G. A. Meehl (2012), An overview of CMIP5 and the experiment design. *Bull. Am. Meteorol. Soc. 93*, 485–498.

Tibaldi S, F. Molteni (1990), On the operational predictability of blocking. *Tellus 42A*, 343-365

Tiedtke, M. (1989), A comprehensive mass flux scheme for cumulus parameterization in large-scale models. *Mon. Weather Rev.*, *117*, 1779-1800.

Thomas, M., J. Sündermann, and E. Maier-Reimer (2001), Consideration of ocean tides in an OGCM and impacts on subseasonal to decadal polar motion excitation, *Geophys. Res. Lett.*, *28*, 2457–2460.

Tsunogai, S., S. Watanabe, and T. Sato, (1999), Is there a continental shelf pump for the absorption of atmospheric CO2?, *Tellus B, 51*, 701–712.

Valcke, S., A. Caubel, D. Declat and L. Terray, (2003), OASIS3 Ocean Atmosphere Sea Ice Soil User's Guide, *Technical report TR/CMGC/03-69, CERFACS, Toulouse, France*.

van der Zee, C., and L. Chou, (2005), Seasonal cycling of phosphorus in the Southern Bight of the North Sea, *Biogeosciences, 2,* 27–42

Wanninkhof, R. (1992), Relationship between wind speed and gas exchange over the ocean, *J. Geophys. Res., 97*, 7373–7382.

Weedon, G. P., S. Gomes, P. Viterbo, W. J. Shuttleworth, E. Blyth, H. Österle, J. C. Adam, N. Bellllouin, O. Boucher, M. Best (2011), Creation of the WATCH Forcing Data and Its Use to Assess Global and Regional Reference Crop Evaporation over Land during the Twentieth Century. *J. of Hydrometeorology, 12***,** 823-848

Wetzel, P. (2004), Interannual and Decadal Variability in the Air-Sea Exchange of CO2 – a Model Study, *Ph.D. thesis*, 127 pp. Available at http://www.mpimet.mpg.de/fileadmin/publikationen/erdsystem_07.pdf.

Zebiak, S. E. and M. A. Cane (1987), A model El Nino - Southern Oscillation. *Mon. Wea. Rev., 115,* 2262¬ 2278.

Zhang, J. L. and D. A. Rothrock (2003), Modeling global sea ice with a thickness and enthalpy distribution model in generalized curvilinear coordinates, *Mon. Weather Rev., 131*, 845-861.

Tables:

	Other models	this study
Primary production	24-49[1]	49
Export production	5.0-7.99[1]	6.5
Carbon uptake ocean	1.5-2.2[2]	1.6

Table 1: Globally integrated carbon fluxes in PgC/yr averaged over the period 1990-1999. The values are derived from an ECHAM forced simulation.
[1] Steinbacher et al., 2010.
[2] Orr et al., 2001.

List of Figures:

Fig.1 Coupling schema. Red color denotes the prescribed forcing used as lateral boundary conditions for REMO and as surface forcing for MPIOM in the uncoupled area. The workflow of heat, momentum and mass fluxes from the atmosphere (REMO) to the ocean (MPIOM) in the coupled area is marked with green. The data flow from MPIOM to REMO is marked with blue.

Fig.2. Grid configuration; the red rectangle contains the coupled domain, in the ocean/sea ice model grid (black lines) only every 15th line is shown.

Fig. 3 Annual mean globally integrated sea to air carbon flux for coarse grid (black curve) and fine grid (red line). For more details see text.

Fig. 4 Mean North Atlantic (30W-10E; 30N-65N) trends in dissolved nitrate diagnosed from the coarse resolution run at different depths. Black: ocean surface, red: 550m, blue: 1500m, green: 3500m.

Fig. 5 Mean winter and summer sea level pressure (1980-1999). ERA-INTERIM (a,e) and the differences Model minus ERA-INTERIM: ROM-NCEP (b,f), ROM-ECHAM5 (c,g), ECHAM5/MPIOM (d,h)

Fig. 6 Standard deviation of DJF (1980-1999) band pass filtered (2.5-7 days) 500 hPa geopotential. ERA-INTERIM (a), ROM-NCEP (b), ROM-ECHAM (c), ECHAM5/MPIOM (d). Winter (e) and Summer (f) relative blocking frequency [after Tibaldi and Molteni,1990] calculated on daily basis. To calculate the blocking index, geopotential simulated by ROM was merged into global geopotential field obtained from corresponding driving model, i.e. ROM-NCEP was merged into NCEP and ROM-ECHAM into ECHAM5.

Fig. 7 Mean winter (upper) and summer (lower) 2m temperature (1980-1999). ERA-INTERIM (a,e) and the differences Model minus ERA-INTERIM: ROM-NCEP (b,f), ROM-ECHAM5 (c,g), ECHAM5/MPIOM (d,h).

Fig. 8 Mean WFD/HOAPS winter and summer (1980-1999) total precipitation (a,e) and the differences Model minus WFD/HOAPS: ROM-NCEP (b,f), ROM-ECHAM5 (c,g), ECHAM5/MPIOM (d,h). Missing HOAPS data are coloured with grey. Note that in contrast to Figures 5 and 7 positive biases are indicated in blue and negative in red.

Fig.9 Large European catchments at 0.5° resolution used by HD model.

Fig.10 Catchment averaged precipitation 1980-1999 [m^3/s]. Baltic Sea catchment (a), Elbe (b), Danube (c), Northern Dvina (d), Rhine (e), Volga (f).

Fig.11 Observed and simulated mean annual cycle of river discharge, 1980-1999 [m^3/s]. Baltic Sea catchment (a), Elbe (b), Danube (c), Northern Dvina (d), Rhine (e), Volga (f).

Fig. 12 Mean (1980-1999) sea level. AVISO data [Schaeffer et al., 2012] (a), ECHAM5/MPIOM (b), ROM-NCEP (c), ROM-ECHAM5 (d).

Fig. 13 Mean (1980-1999) barotropic stream function. ROM-NCEP (a), ROM-ECHAM5 (b), ECHAM5/MPIOM (c)

Fig. 14 Mean Atlantic meridional overturning streamfunction averaged for 1980-1999 (Sv).

Fig. 15 Observed (a) and modelled (b) M_2 tidal maps. Co-tidal lines are with 30^o interval. Mean 0-200 m passive tropical tracer concentration in the simulation with tides (c) and its relative change (%) from the simulation without tides (d). Winter/Spring (e) and Summer/Autumn (f) 2 m temperature difference between the simulations with and without tidal forcing

Fig. 16 Mean (1980-1999) sea surface temperature (SST) WOA2009 climatology (a) and differences Model minus WOA2009: ROM-NCEP (b), ROM-ECHAM5 (c), ECHAM5/MPIOM (d).

Fig. 17 Mean (1980-1999) sea surface salinity (SSS) and freshwater flux from WOA2009 climatology (a),and differences Model minus WOA2009: ROM-NCEP (b), ROM-ECHAM5 (c), ECHAM5/MPIOM (d). ROM-ECHAM5 natural (non-corrected) freshwater flux to the ocean (e) and freshwater flux correction due to salinity restoring (f)

Fig. 18 Annual mean sea ice extent in the GIN Sea (black) and SST in North and Baltic Seas (blue) (a). Thick lines – 5 years running mean. (b) and (c) are the composites of 2m temperature (T2M) anomalies calculated for 1920-2000. (b): mean T2M anomalies for the years when GIN Sea ice extent is lower than its multiyear mean minus standard deviation, (c): mean T2M anomalies for the years when GIN Sea ice extent is larger than its multiyear mean plus standard deviation.

Fig.19 Mean 1980-1999 February (a,b,c,d) and September (e,f,g,h) sea ice thickness for PIOMAS (a,e), ROM-NCEP (b,f), ROM-ECHAM5 (c,g) and ECHAM5/MPIOM (d,h).

Fig.20 Observed WOA2009 (a) and modelled 1980-1999 yearly mean surface phosphate concentration. ROM-NCEP (b) and ROM-ECHAM5 (c).

Fig.21 Vertically integrated annual mean primary production. SeaWiFS ; [from Behrenfeld et al., 2006] (a) and ROM-NCEP (b). Only areas with a continuous record of observations (1998-2006) are shown

Fig.22 Observed WOA2009 (a,b) and modelled Atlantic zonally averaged phosphate and nitrate concentration. ROM-ECHAM5 (c,d) and ROM-NCEP (e,f).

Fig.23 (a) Correlation between modelled and satellite based estimates for net primary production (SeaWiFS; [Behrenfeld et al., 2006; Behrenfeld and Falkowski, 1997]). Displayed is the correlation of monthly mean values between 1998 and 2006. (b) Month in which the maximal production occurs (averaged over the period 1950-2000 for the ROM-ECHAM5 historical run).

Fig.24 Correlation map between SeaWifs estimated production and ROM-NCEP simulation: yearly mean production (a) and multiyear March production (b). The considered time frame is 1998 – 2006. Note: Only grid points with a continuous record of ocean color data are depicted.

Fig.25 NO_3 analysis and salinity analysis for the North Sea. Blue ECHAM6/MPIOM, red: ROM-NCEP, black: ROM-ECHAM5. For the analysis of NO_3 observations were taken from Marine Environmental Data Base (MUDAB, http://www.marbef.org/wiki/MUDAB). In total 2073 observation were used distributed over the entire North Sea. About 28 % originate from the upper ten meters of the water column. For salinity analysis observations from the gridded World Ocean Atlas (2013) were employed. Analysis period is 1993 – 2008.

Fig.26 Yearly cycle of temperature in the northern North Sea at 0.95°E; 58.7°N obtained from ECHAM6/MPIOM (a) and ROM-ECHAM5 (b) simulations. An average is shown for the period 1980 -1999.

Fig.27 Various model configurations for ROM: North Atlantic and Northern Europe (a), Arctic (b), South-East Asian (c), West African (d) and Indian Monsoons (e). Black lines – ocean model grid (every 12^{th} grid line), coloured rectangles – coupled areas.

External forcing

surface pressure
temperature
wind velocity
specific humidity
liquid water content

REMO

10m wind velocity
wind stress
2m temperature
2m dew point temperature
total precipitation
downward shortwave radiation
total cloud cover or
downward longwave radiation

surface runoff
drainage

HD

surface runoff
drainage

river runoff

10m wind velocity
wind stress over water
wind stress over sea ice
liquid precipitation
solid precipitation
net shortwave radiation
total heat flux over water
conductive heat flux
residual heat flux

Bulk formulae

10m wind velocity
wind stress over water
wind stress over sea ice
liquid precipitation
solid precipitation
net shortwave radiation
total heat flux over water
conductive heat flux
residual heat flux

OASIS

Uncoupled area

REMO → MPIOM

MPIOM → REMO

MPIOM/HAMOCC

surface temperature
sea ice thickness
sea ice concentration
snow depth
ocean surface velocity
sea ice velocity

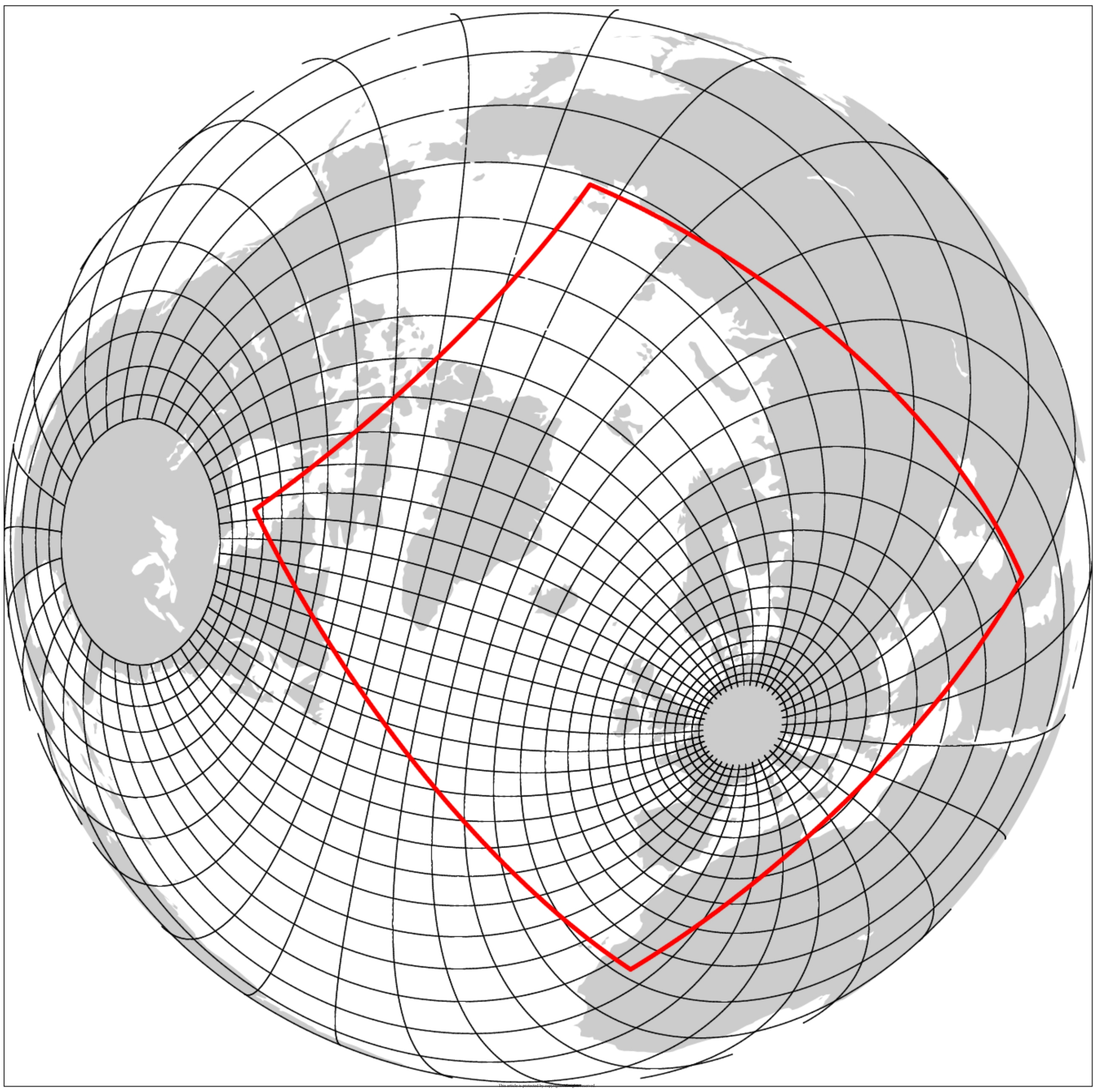

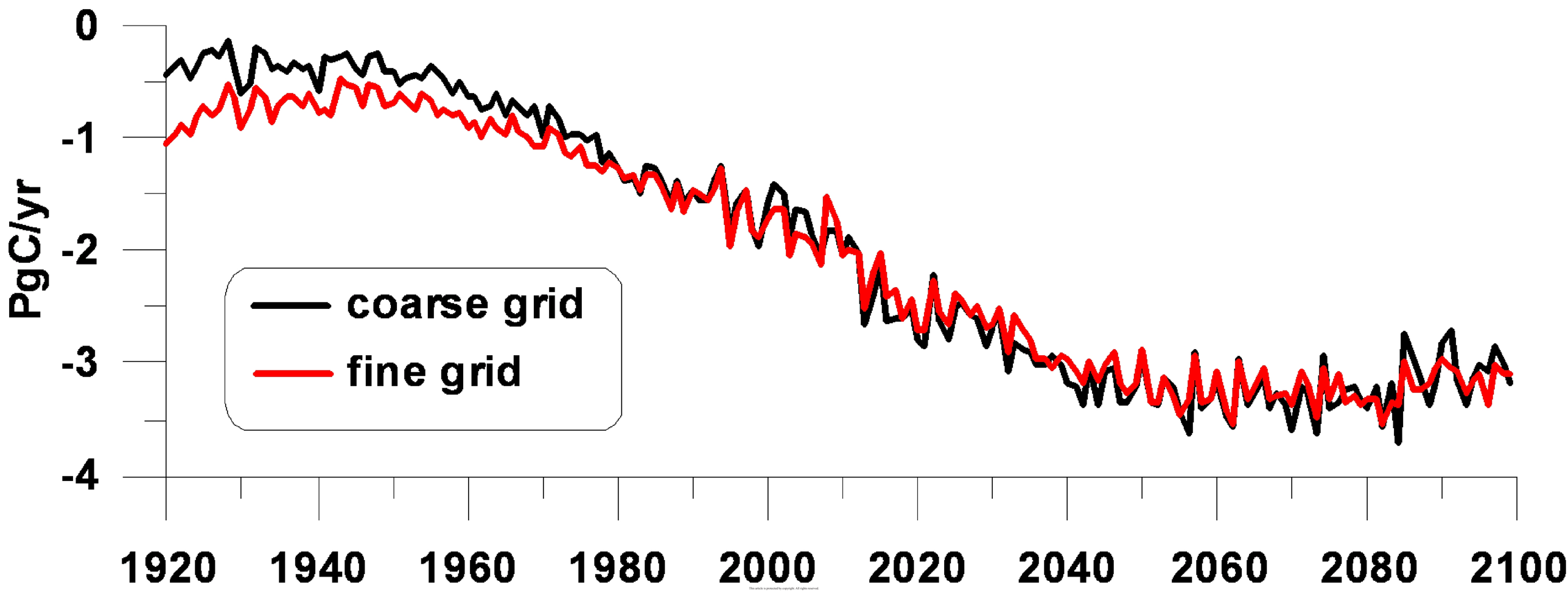

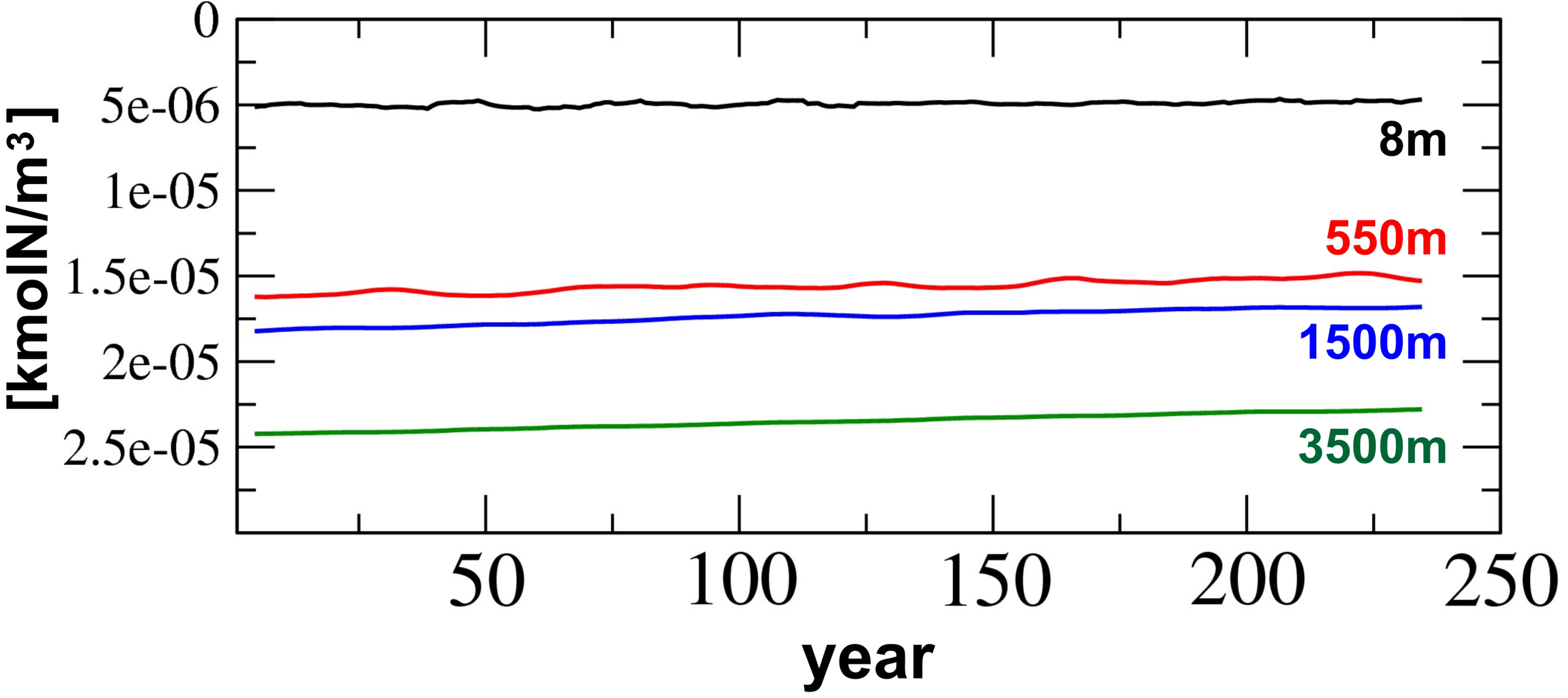

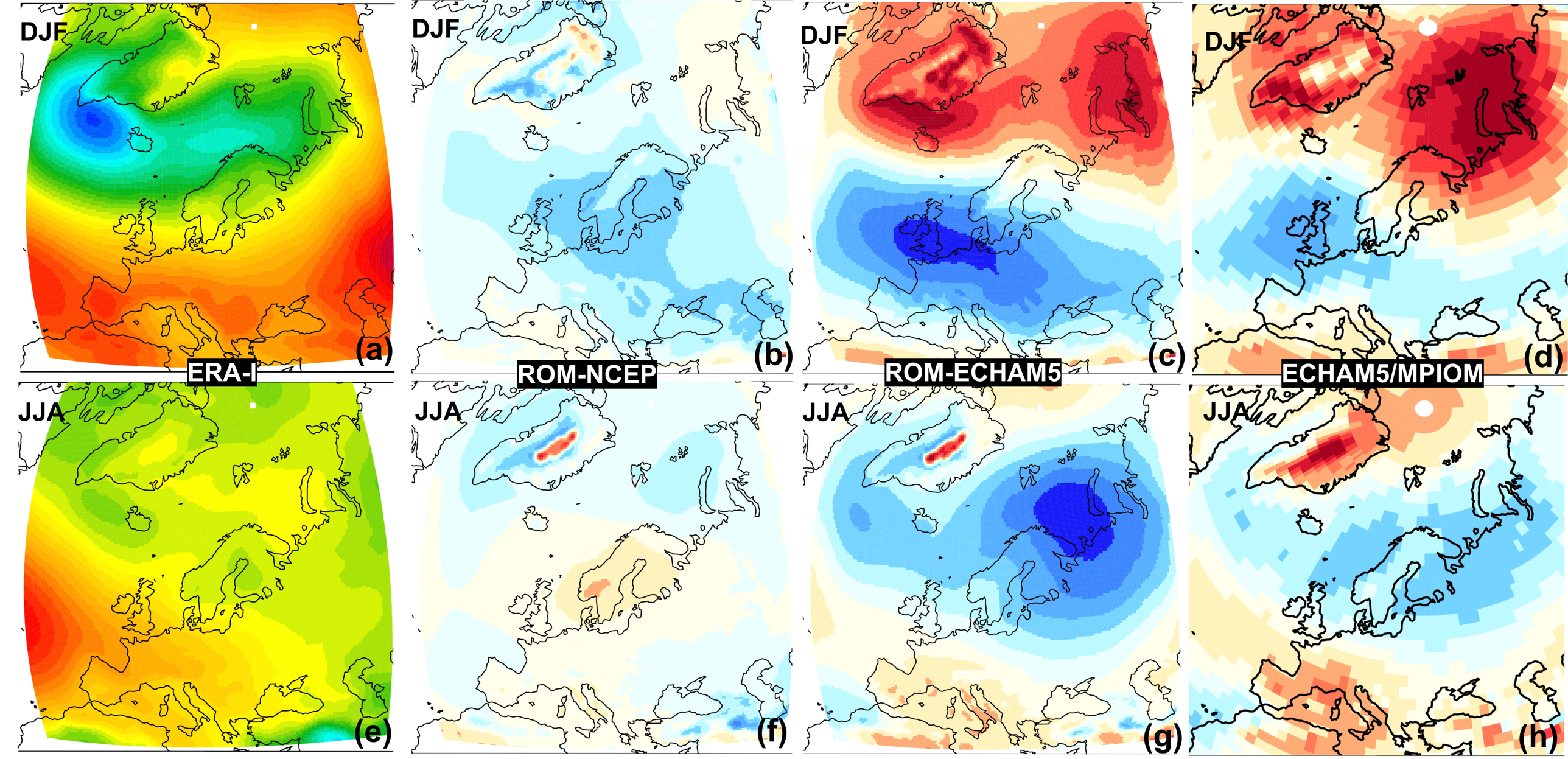

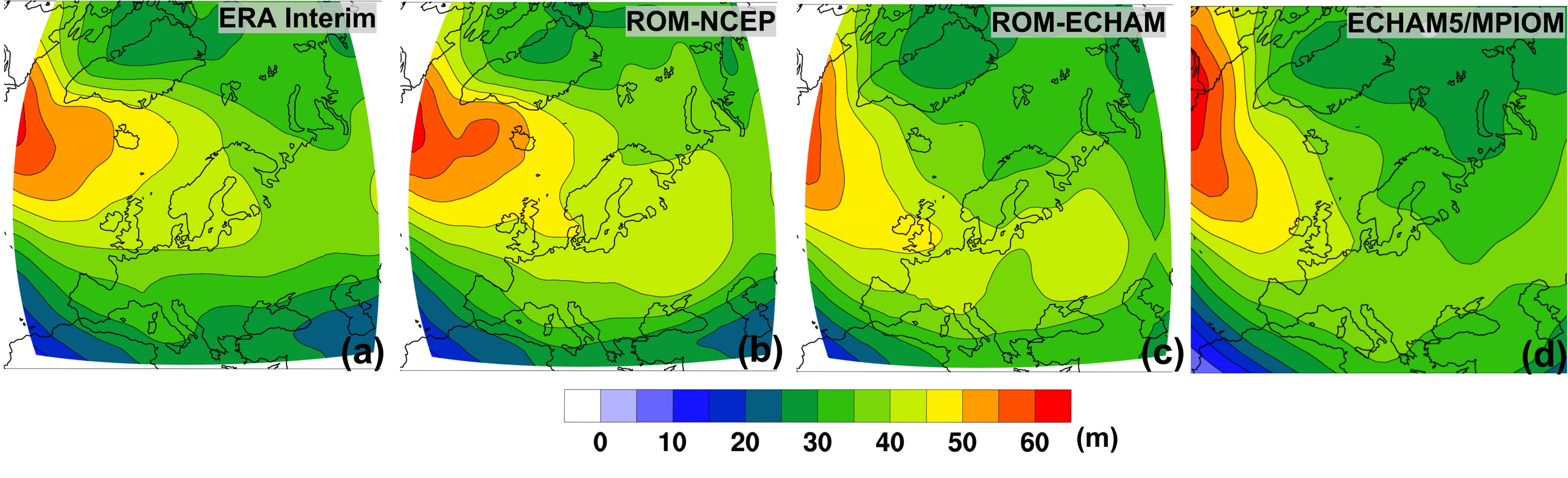

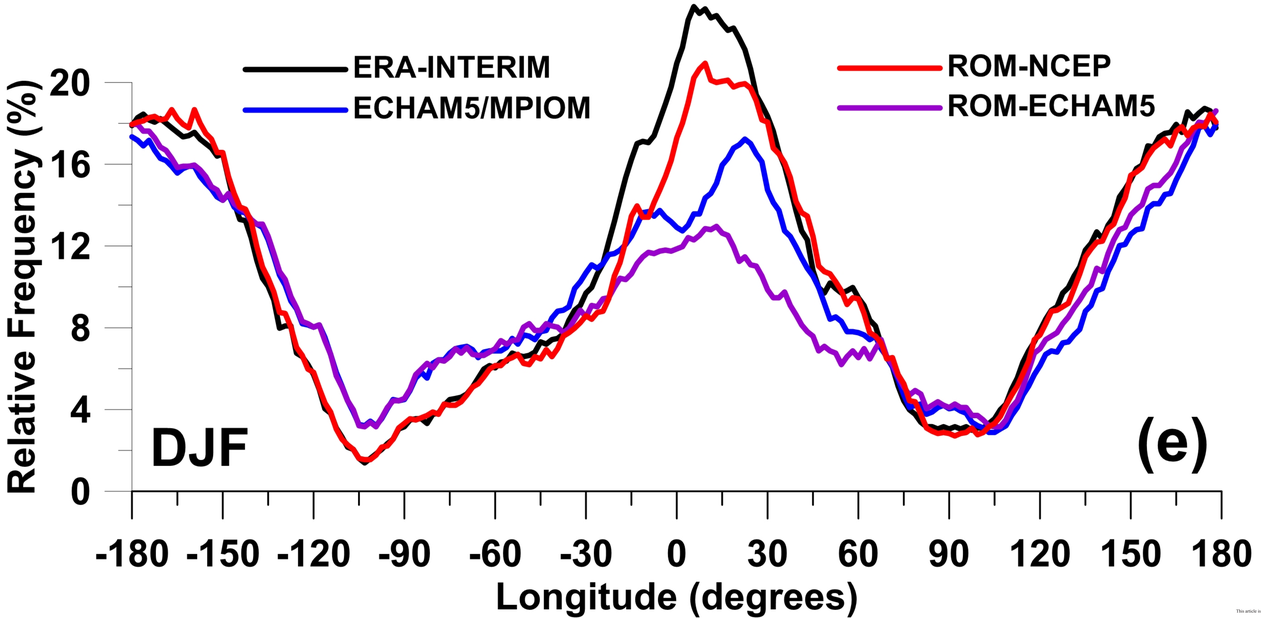

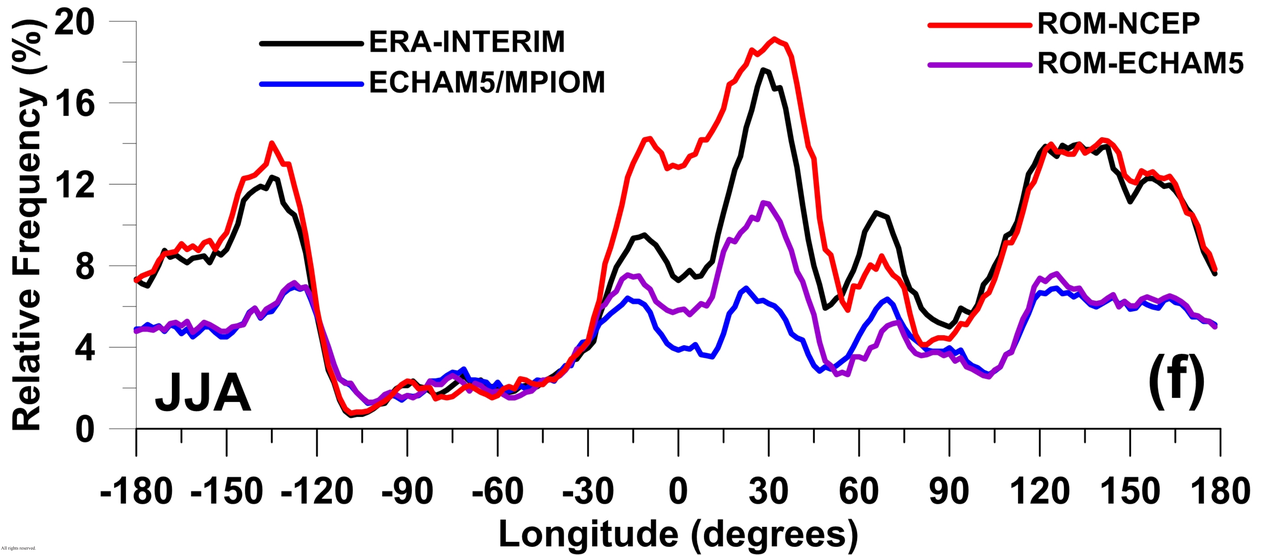

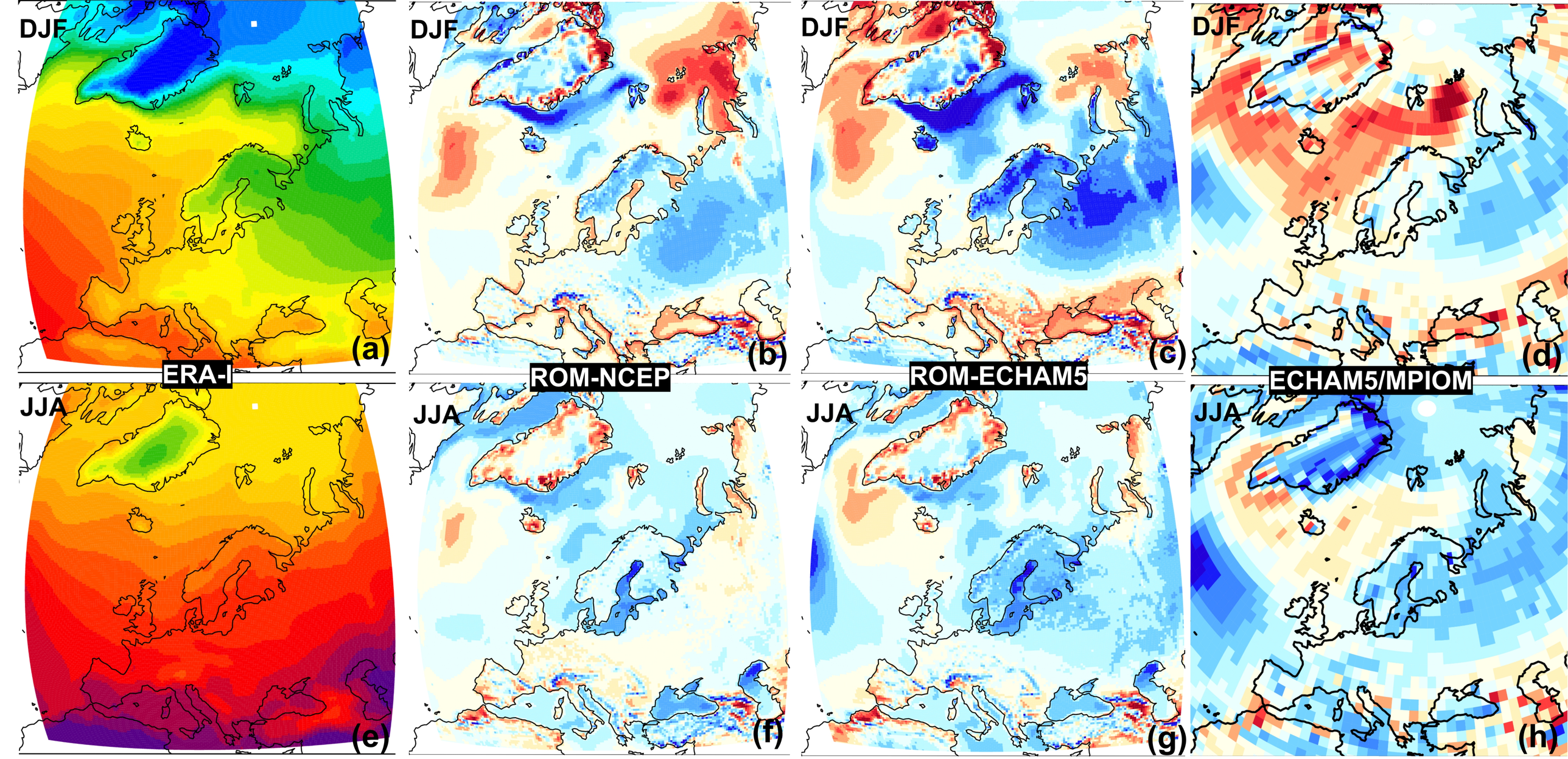

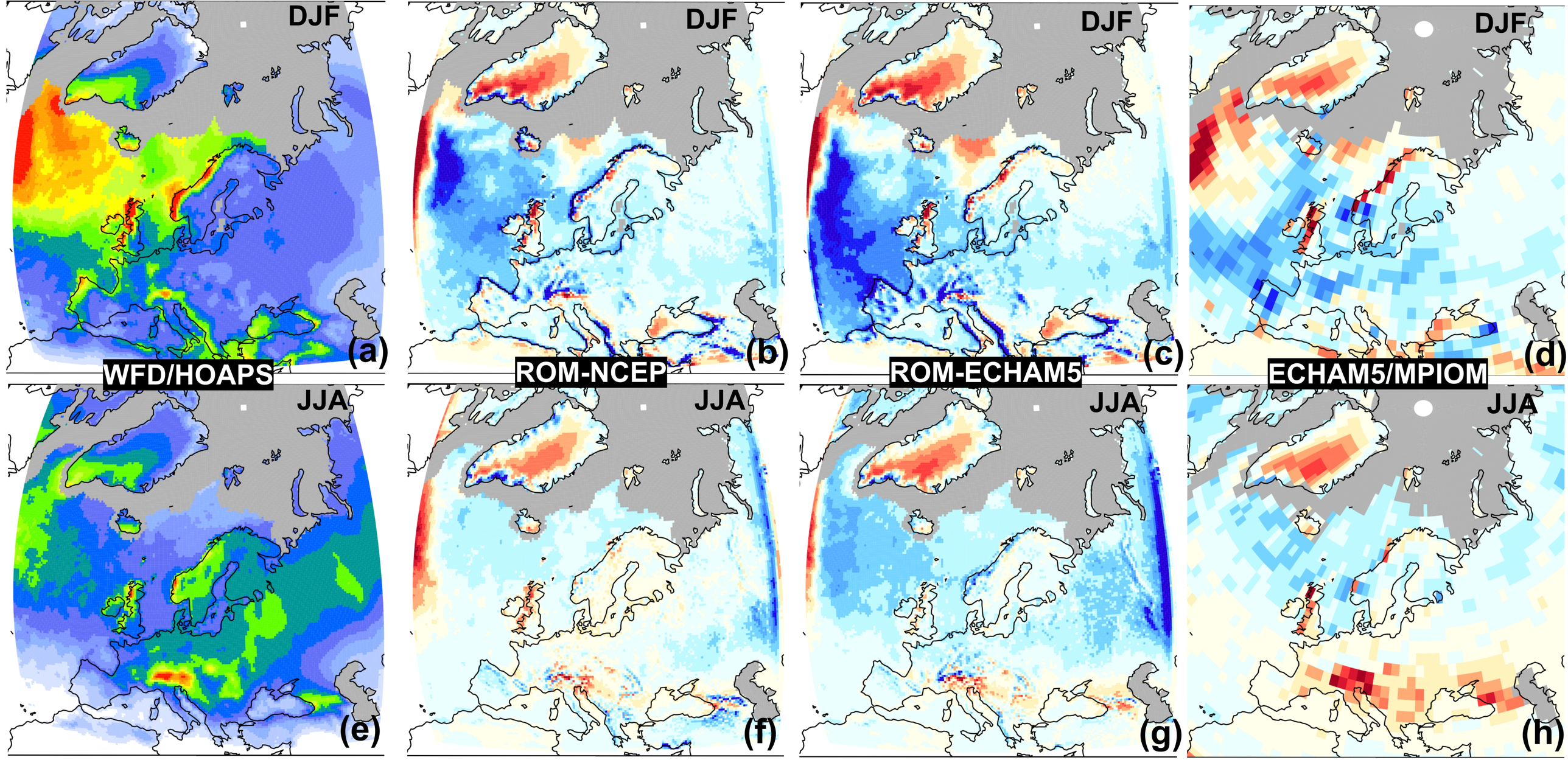

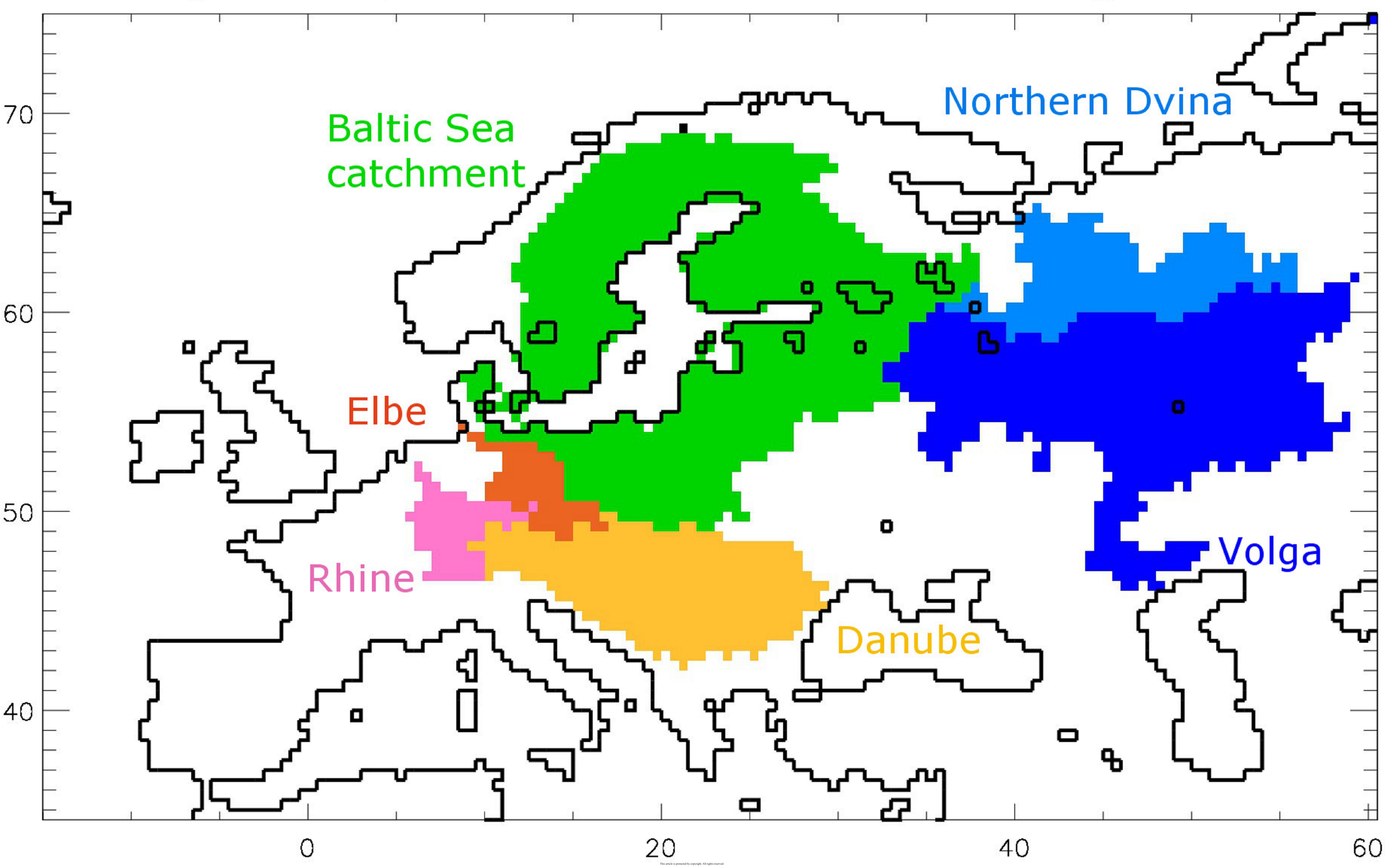

PRECIPITATION
Baltic Sea catchment

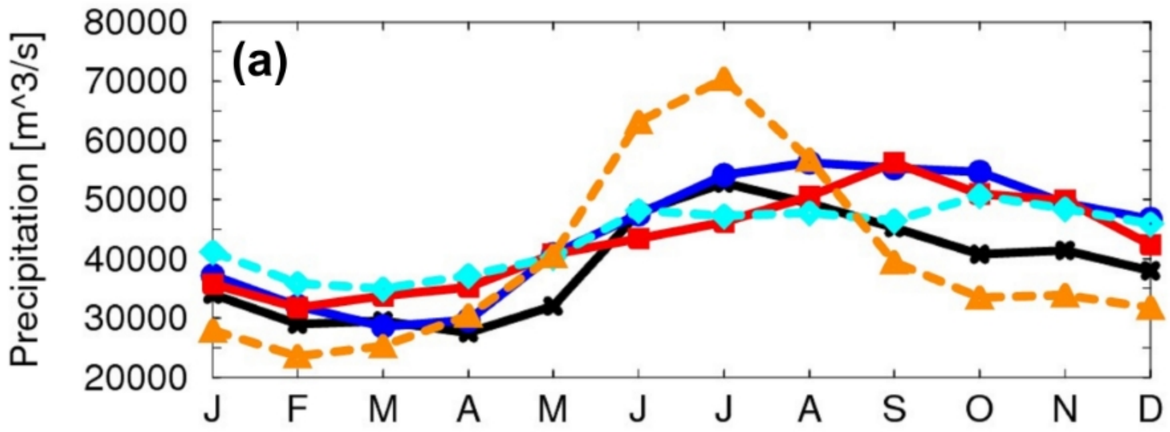

PRECIPITATION
Elbe

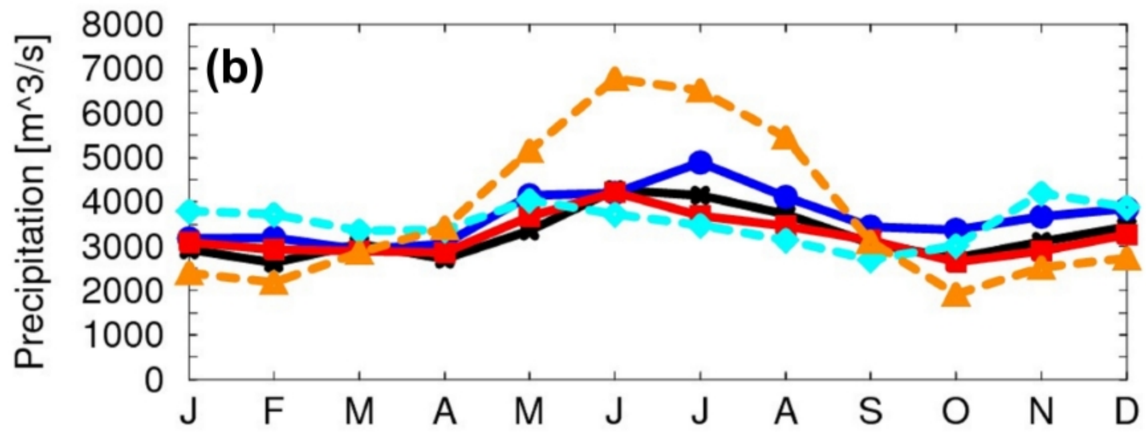

Danube

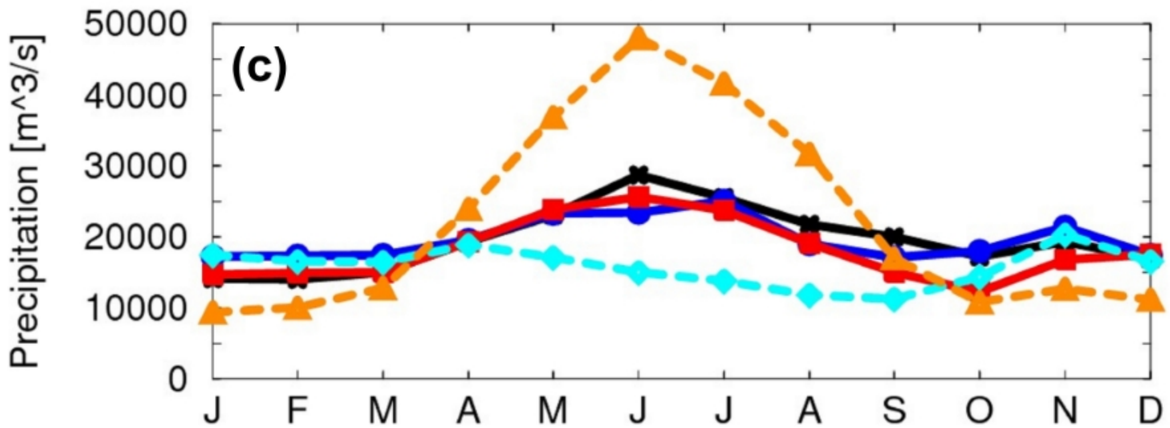

Northern_Dvina

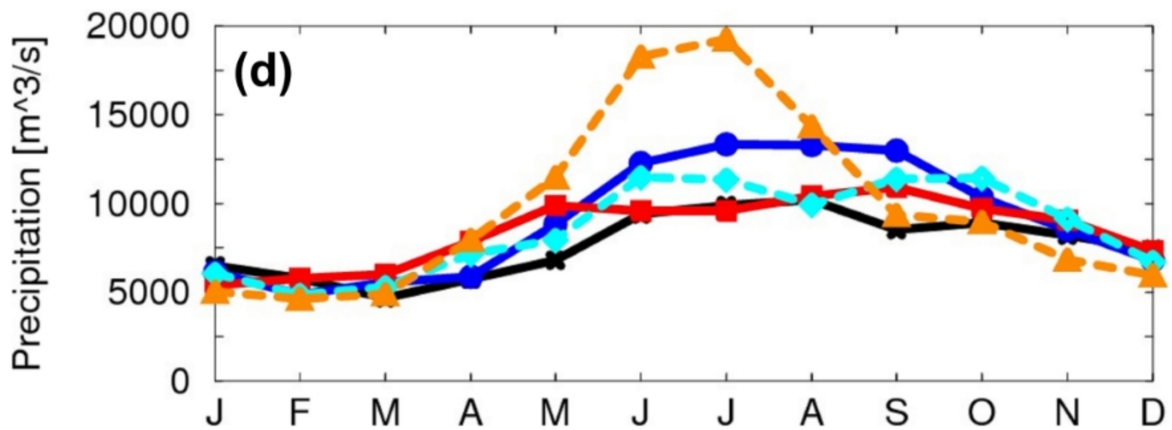

Rhine

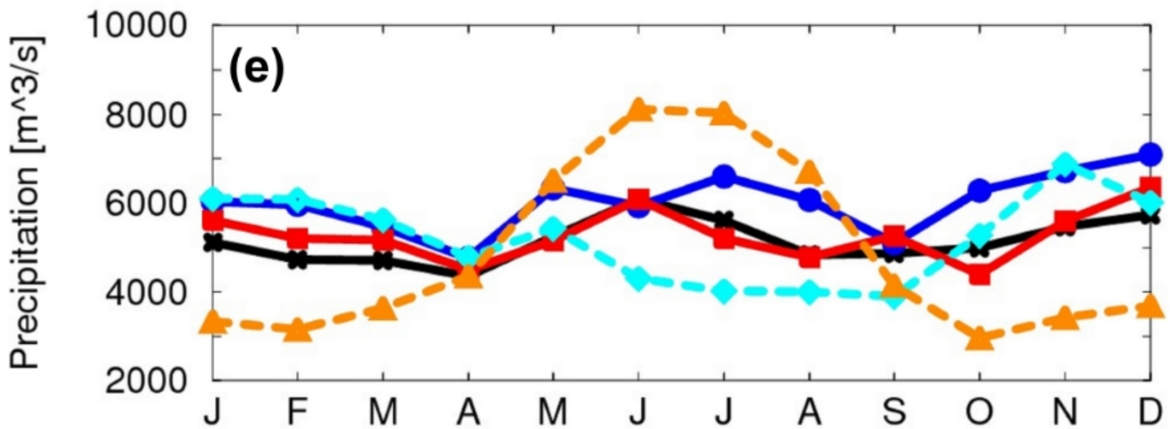

Volga

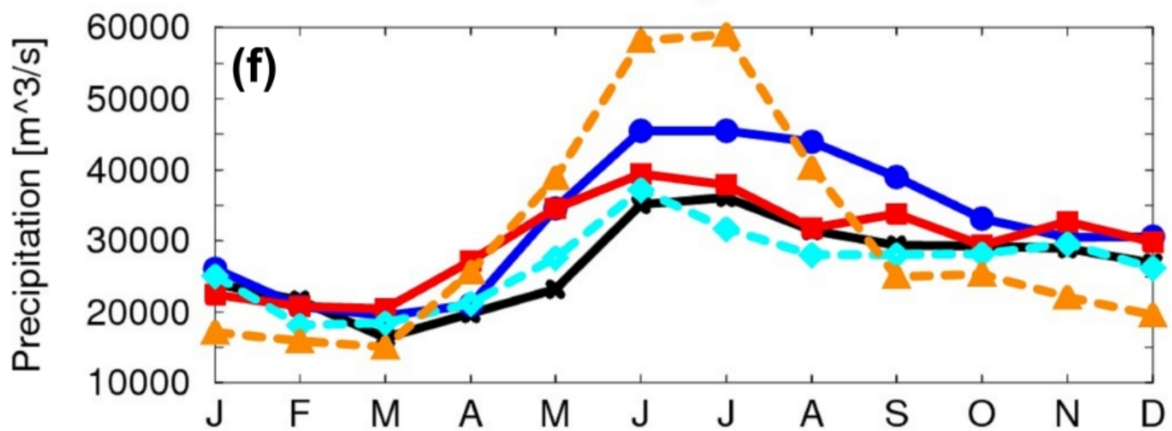

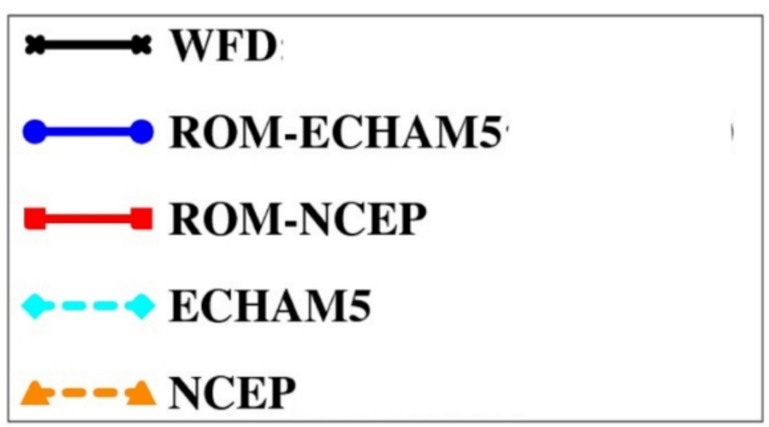

DISCHARGE

Baltic Sea catchment

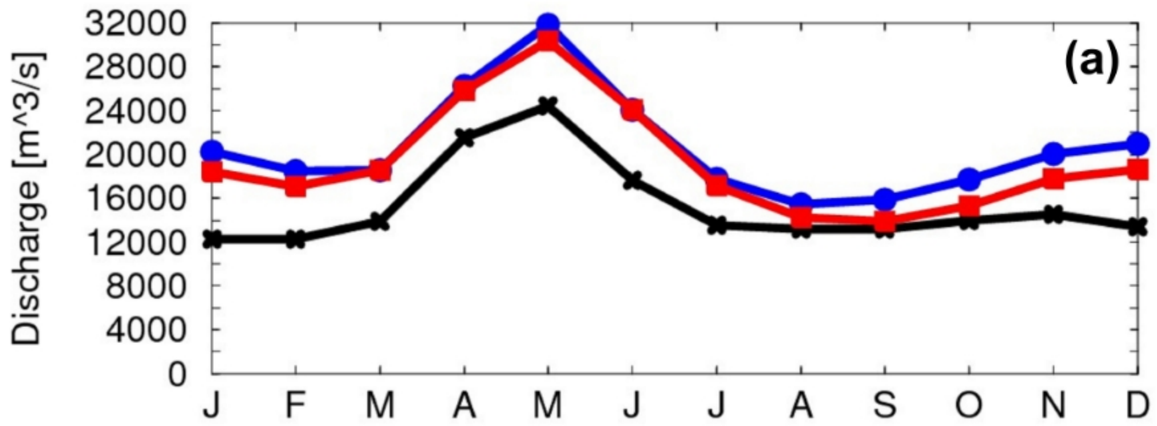

DISCHARGE

Elbe

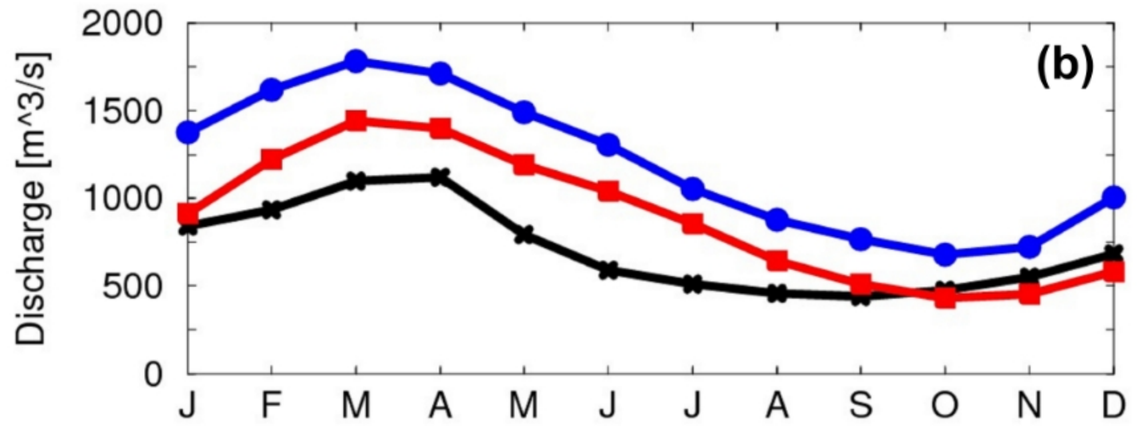

Danube

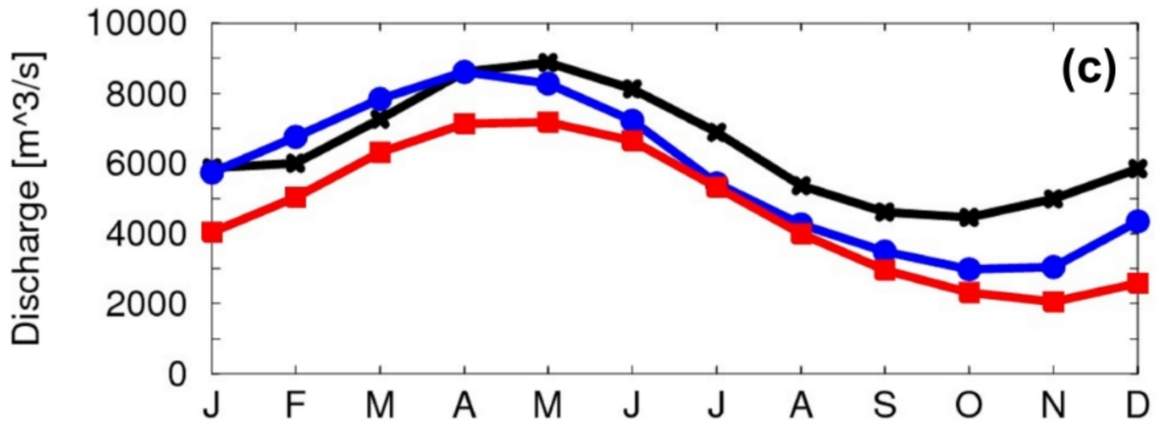

Northern_Dvina

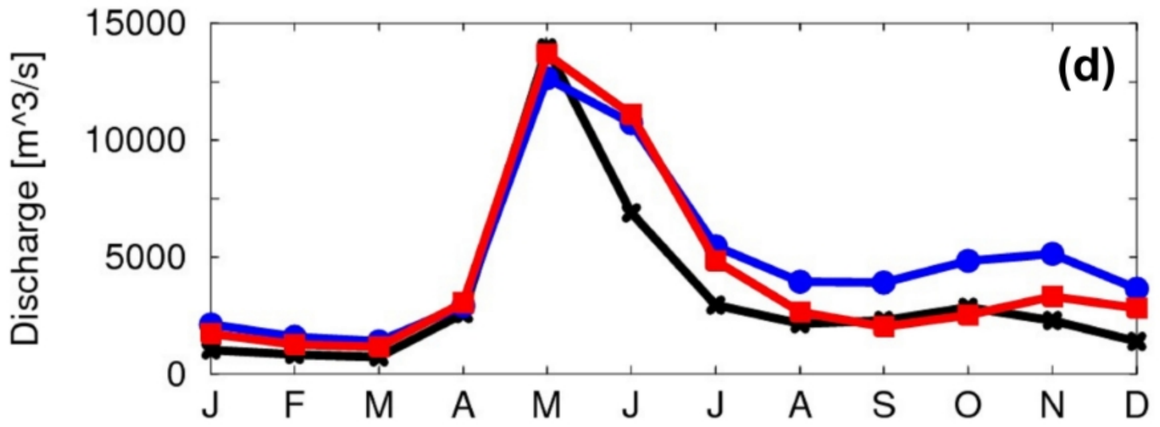

Rhine

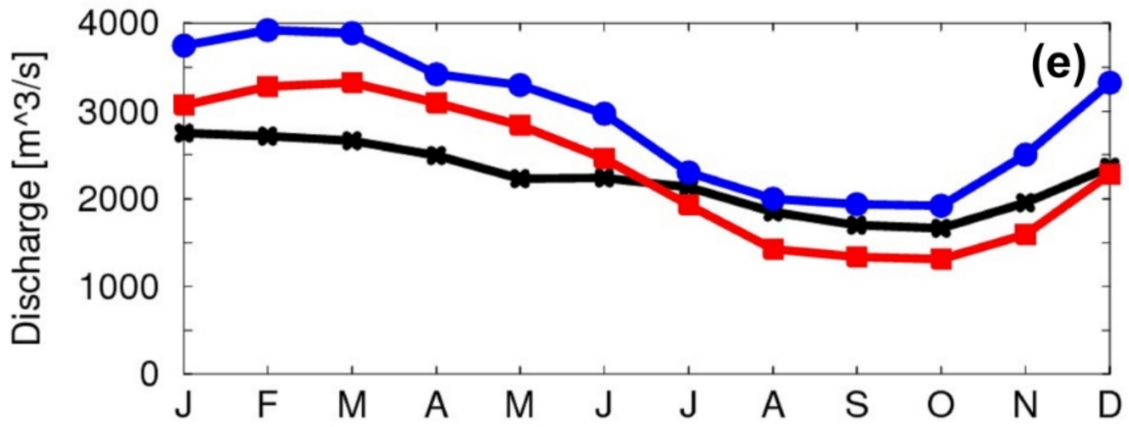

Volga

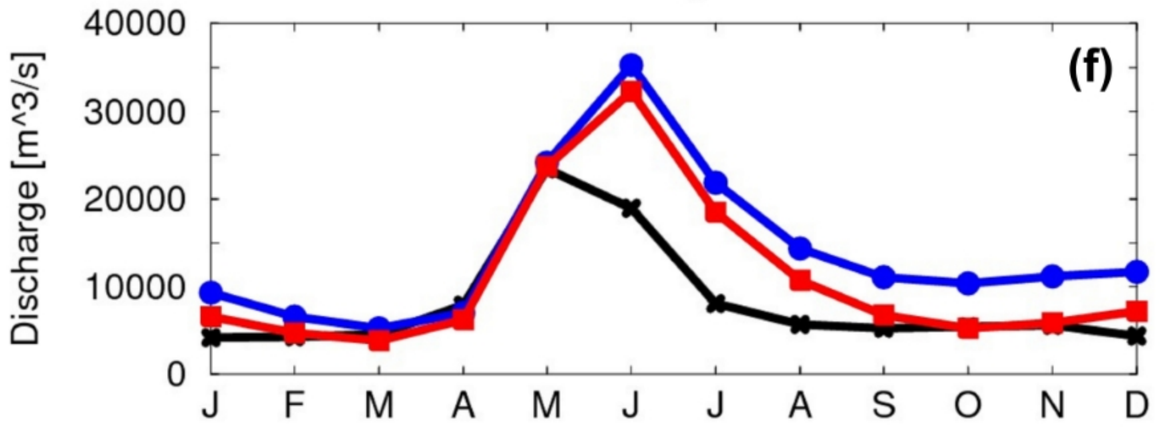

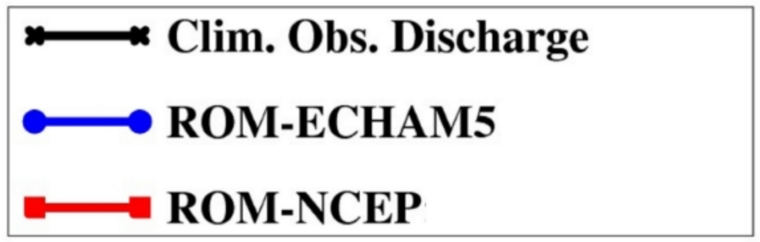

(a)

AVISO

(b)

ECHAM5/MPIOM

(c)

ROM-NCEP

(d)

ROM-ECHAM5

-1.4 -1.2 -1 -0.8 -0.6 -0.4 -0.2 0 0.2 0.4

(m)

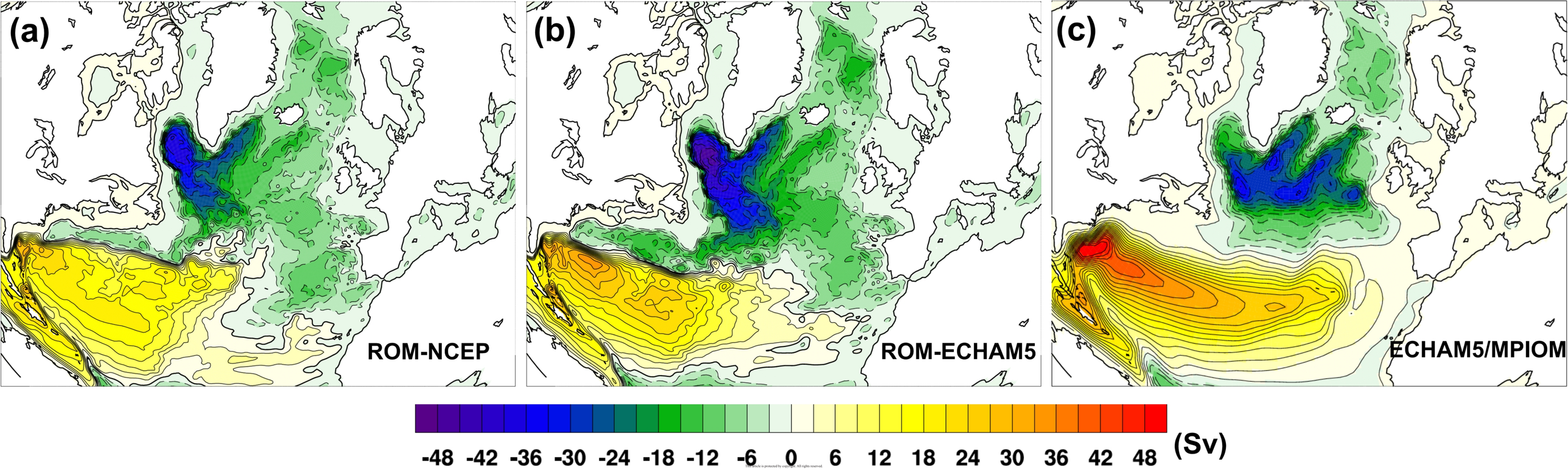

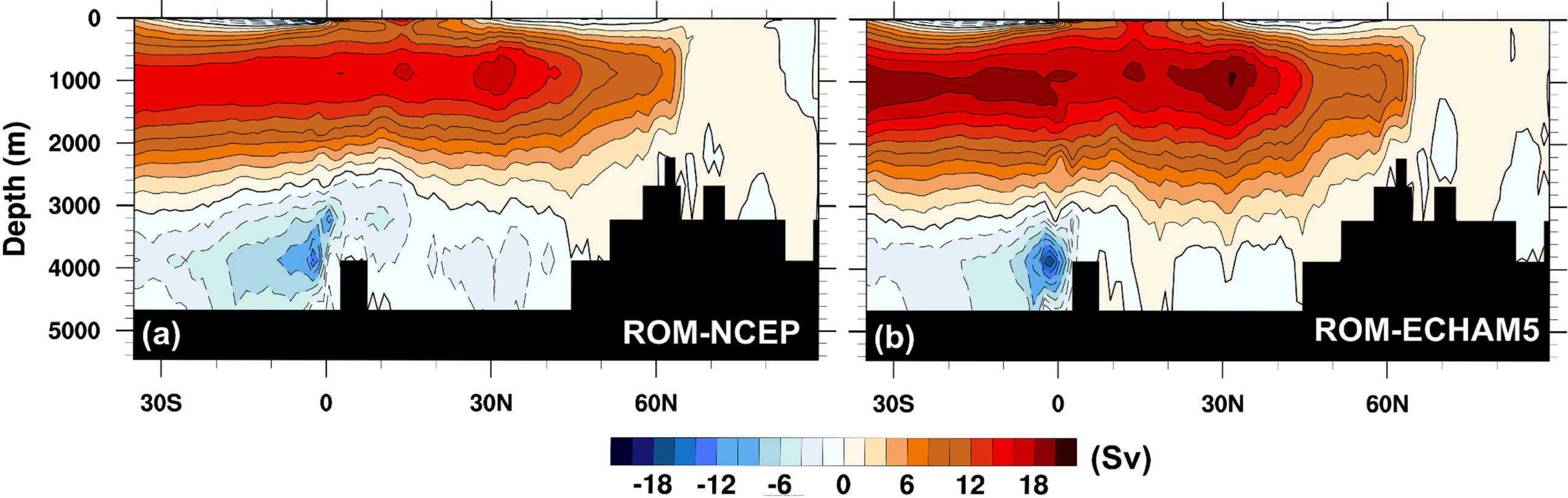
Depth (m)
0
1000
2000
3000
4000
5000
(a)
ROM-NCEP
(b)
ROM-ECHAM5
30S
0
30N
60N
30S
0
30N
60N
-18
-12
-6
0
6
12
18
(Sv)

(a)

(b)

TOPEX/POSEIDON

ROM-ECHAM5

40°N
30°N
20°N
10°N
0°

60°W 45°W 30°W 15°W 0°

0 0.4 0.8 1.2 1.6 2 (m)

(c)

(d)

ROM-ECHAM5

ROM-ECHAM5

0 0.2 0.4 0.6 0.8 1

-20 -10 0 10 20 (%)

(e)

(f)

DJFMAM ROM-ECHAM5

JJASON ROM-ECHAM5

-0.8 -0.6 -0.4 -0.2 0 0.2 0.4 0.6 0.8 (K)

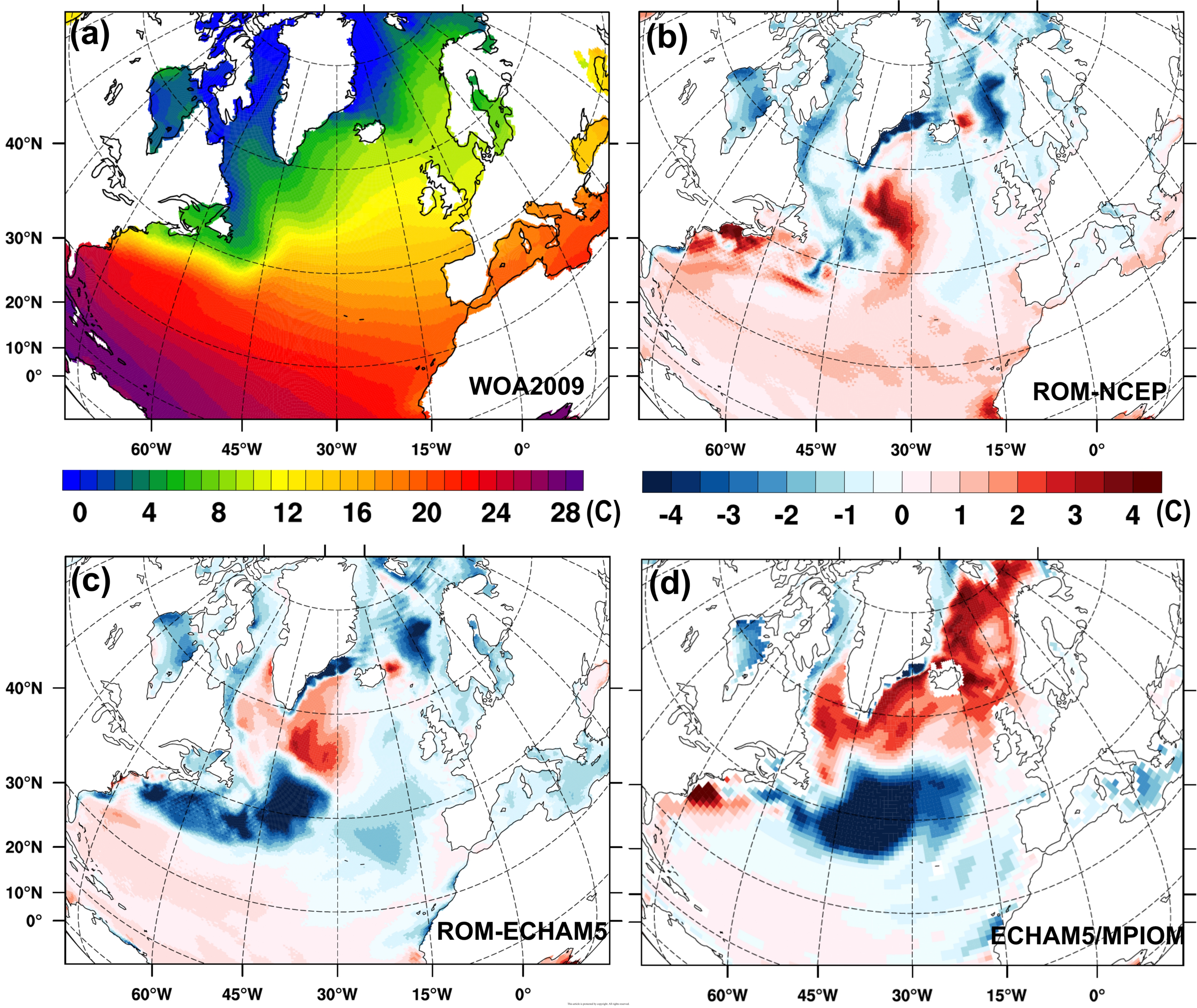

(a)

(b)

(c)

(d)

(e)

(f)

40°N
30°N
20°N
10°N
0°

60°W 45°W 30°W 15°W 0°

WOA2009

ROM-NCEP

ROM-ECHAM5

ROM-ECHAM5

ECHAM5/MPIOM

ROM-ECHAM5

30 31 32 33 34 35 36 37

-2 -1.5 -1 -0.5 0 0.5 1 1.5 2

-5 -4 -3 -2 -1 0 1 2 3 4 5 (mm/day)

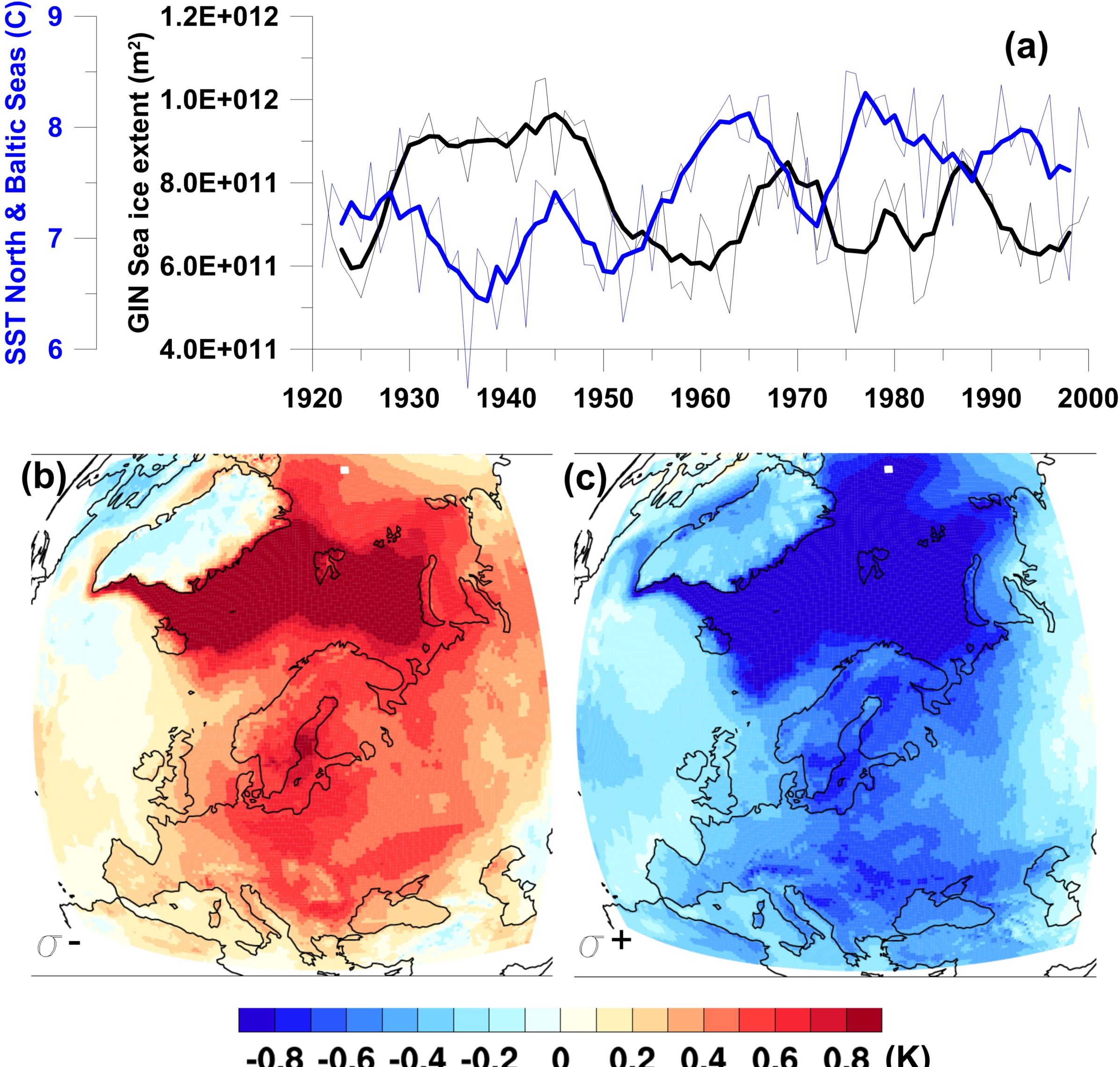

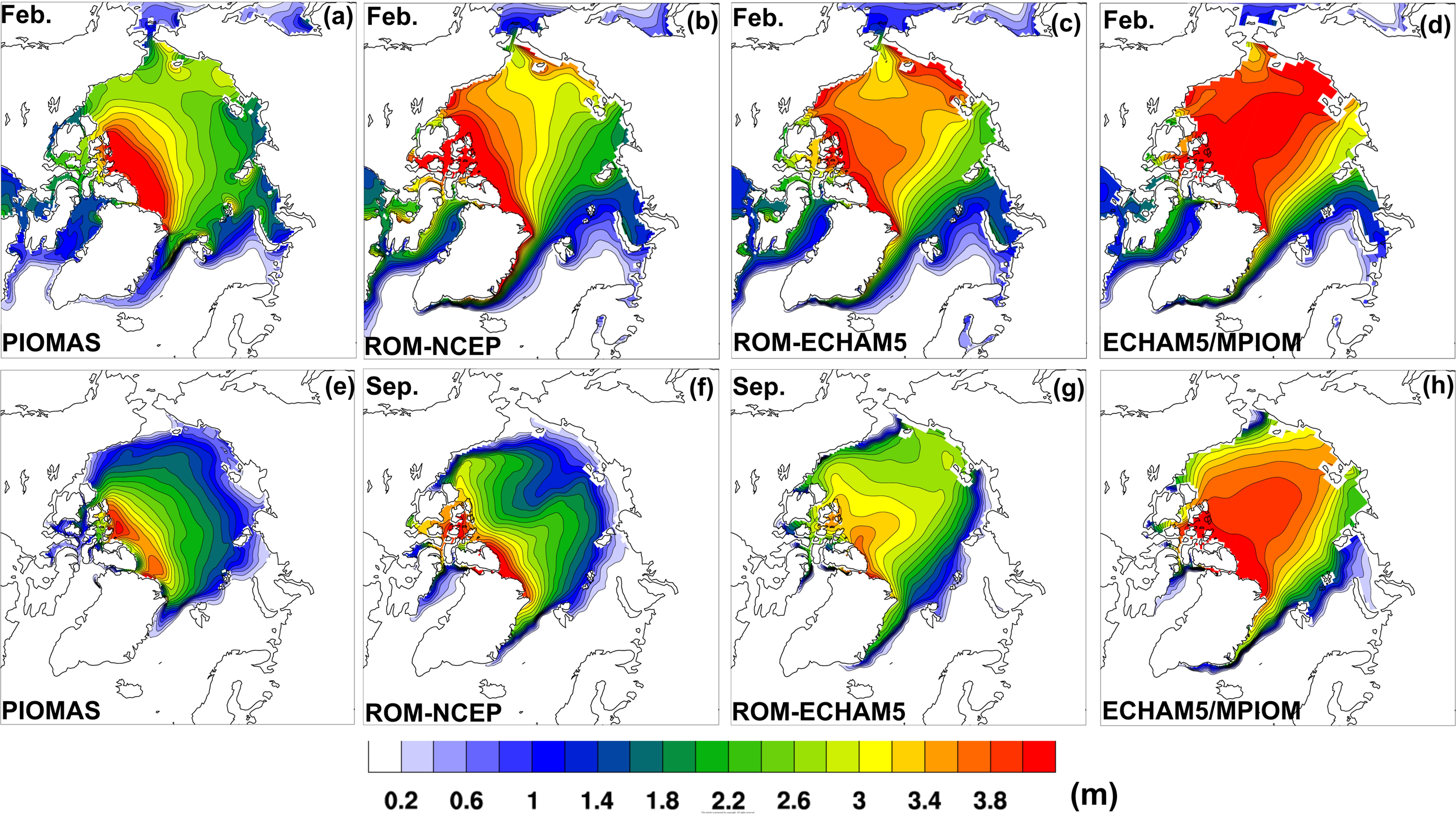
Feb.
(a)
PIOMAS
Feb.
(b)
ROM-NCEP
Feb.
(c)
ROM-ECHAM5
Feb.
(d)
ECHAM5/MPIOM
(e)
PIOMAS
Sep.
(f)
ROM-NCEP
Sep.
(g)
ROM-ECHAM5
(h)
ECHAM5/MPIOM
0.2
0.6
1
1.4
1.8
2.2
2.6
3
3.4
3.8
(m)

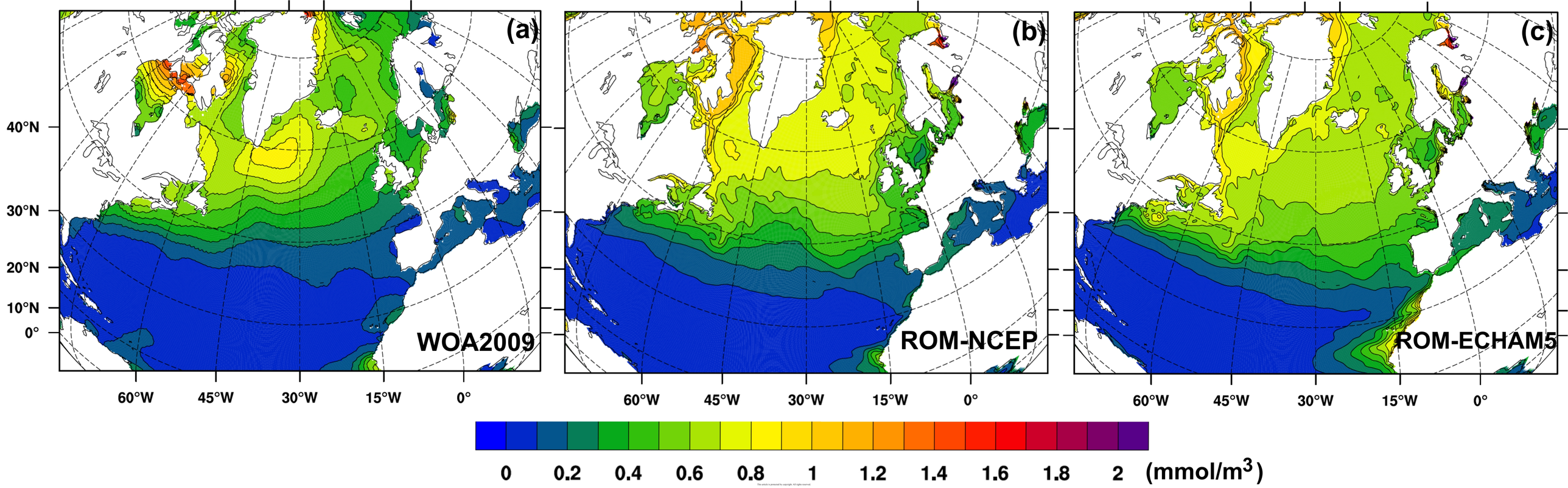
(a)
(b)
(c)
WOA2009
ROM-NCEP
ROM-ECHAM5
40°N
30°N
20°N
10°N
0°
60°W
45°W
30°W
15°W
0°
0
0.2
0.4
0.6
0.8
1
1.2
1.4
1.6
1.8
2
(mmol/m3)

(a)

60°N
30°N
0°
30°S
60°S

180° 135°W 90°W 45°W 0° 45°E 90°E 135°E 180°

SeaWiFS

(b)

60°N
30°N
0°
30°S
60°S

180° 135°W 90°W 45°W 0° 45°E 90°E 135°E 180°

ROM-NCEP

100 500 900 1300 1700 2100 mgC/m^2/day

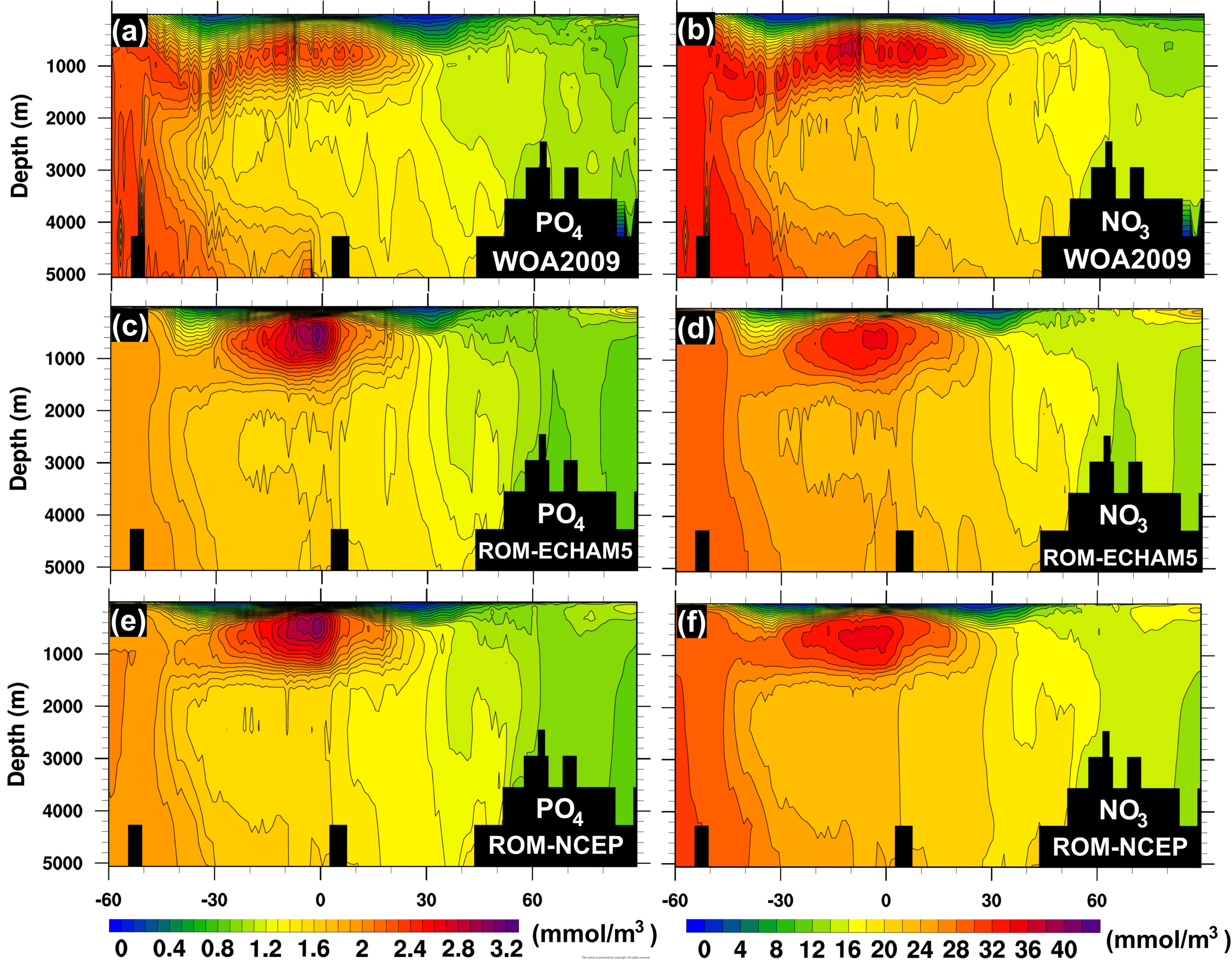

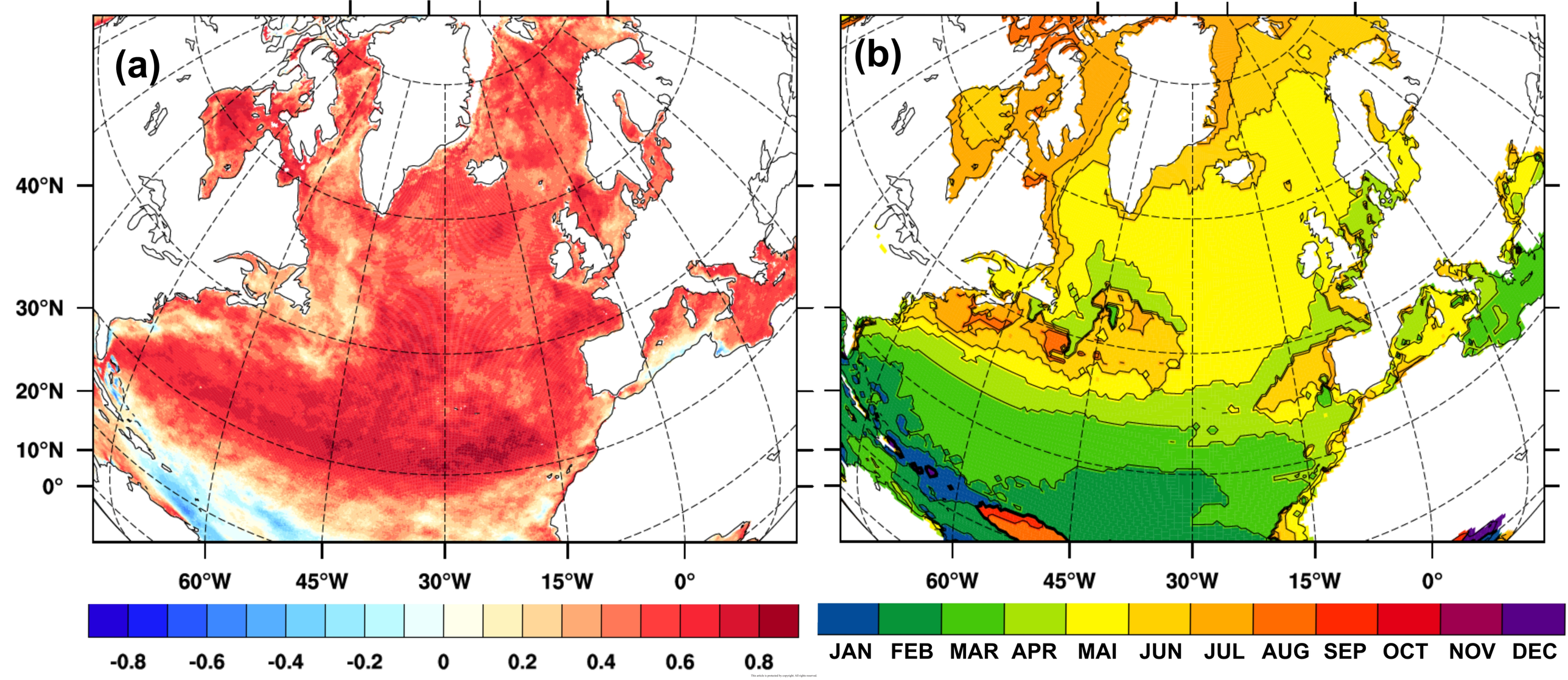

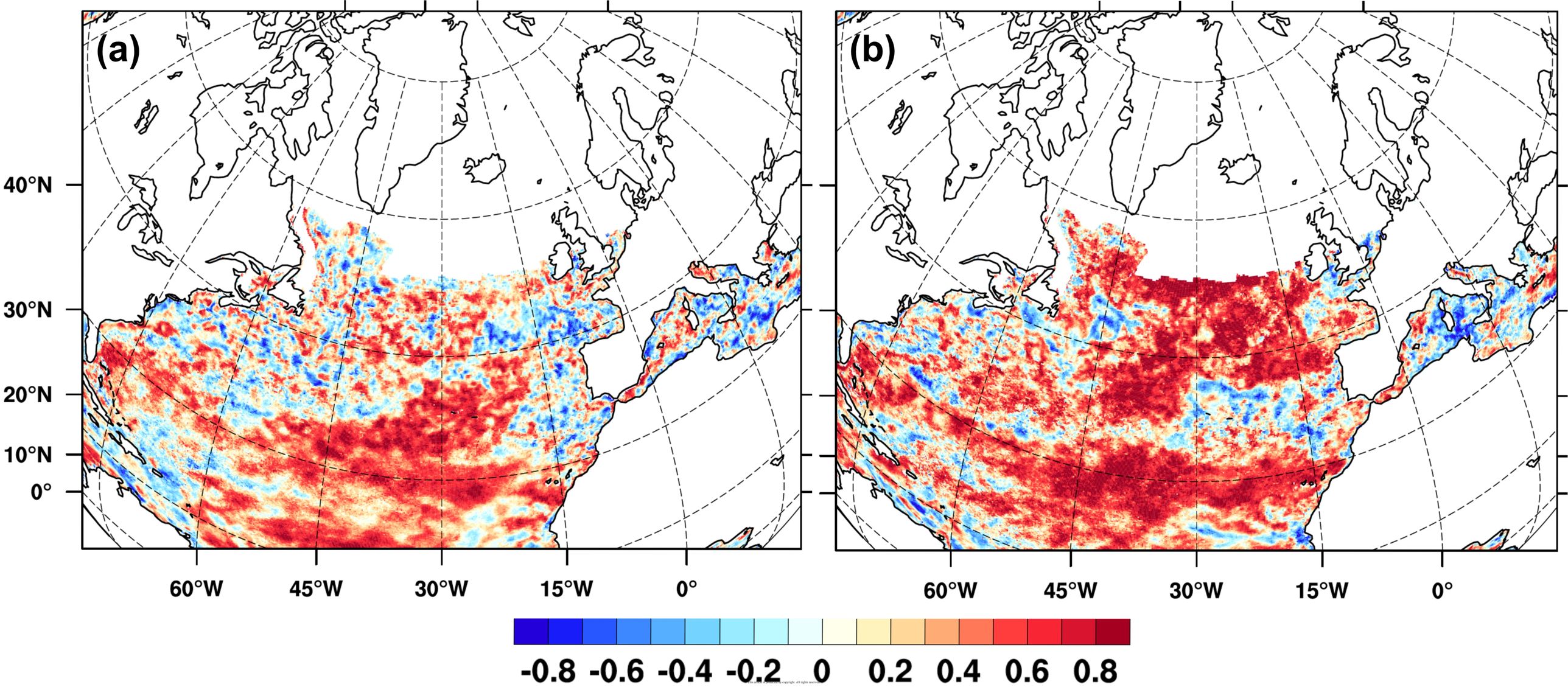
(a)
(b)
40°N
30°N
20°N
10°N
0°
60°W
45°W
30°W
15°W
0°
-0.8 -0.6 -0.4 -0.2 0 0.2 0.4 0.6 0.8